UNIVERSITY OF ANTIOQUIA

Master Science Program - Physics

Research work

RANDOM FLUCTUATIONS IN NUCLEAR REACTORS: STOCHASTIC POINT KINETICS EQUATIONS WITH TWO-ENERGY GROUPS

Senior advisor
Prof. Johan Mazo Zuluaga, Ph.D.
Consultant
Prof. Rodrigo Henao Henao, Ph.D.

Candidate
Daniel E. Cedeño Girón

May 2022

RANDOM FLUCTUATIONS IN NUCLEAR REACTORS: STOCHASTIC POINT KINETICS EQUATIONS WITH TWO-ENERGY GROUPS

by
Daniel E. Cedeño Girón

Submitted as partial requirement to obtain the degree of

MASTER SCIENCE IN PHYSICS

University of Antioquia
Medellín, Colombia
2022

ACKNOWLEDGMENTS

I would like to thank the entire Physics Institute of the University of Antioquia, in especial Dr. Johan Mazo Zuluaga and Dr. Rodrigo de Jesús Henao Henao for guiding and advising me throughout my graduate studies. In addition, to Dr. León Alexander Valencia Henao from the Institute of Mathematics for his criticism and effort. I also thank the *Estudiante Instructor* program at the University of Antioquia for its training space and financial support. Also, I would like to thank Dr. Abdallah A. Nahla from the Mathematics Department of Tanta University for his willingness to collaborate and advise. I would also like to thank the referees for their suggestions and comments, which undoubtedly contributed to improve the quality of this document. Last, but certainly not least, to my mother, who has always shown me her love, support, and sacrifice.

ABSTRACT

Dynamics of a nuclear reactor is described on the basis of the mean values of the neutron-nucleus interactions. The Point Kinetics equations model uses these values to describe the time evolution of the neutron population in homogeneous reactors. Significant random fluctuations of the neutron population are observed at the reactor startup and shutdown, caused by the statistical nature of the system and due to unexpected events, such as sub-cooled boiling, pressure fluctuations, and mechanical vibrations of control and fuel rods, among others. The Point kinetics equations cannot describe these fluctuations due to their deterministic nature. An adequate description of the reactor dynamics is achieved through stochastic models, such as the stochastic Point Kinetics equations, which provides accurate information on the mean values and standard deviations of the neutron populations. However, this model considers mono-energetic neutrons, which is far from reality. In addition, the realizations of the stochastic process do not adequately describe the reactor dynamics.

The aim of this study is adding physical rigor to the stochastic model of the Point Kinetics equations by discriminating in energy the neutron population, which determines the probability of interaction with atomic nuclei; and to propose a solution to the problem of the stochastic realizations of the related process. The outcome is a stochastic model with realizations in agreement with reality, and predictions of both the mean values and the standard deviations, which turns out to be in good agreement with experimental and simulated data reported previously. These comparisons show that our stochastic model accurately describes the random behavior of the neutron population in a homogeneous nuclear reactor.

Finally, it is worth mentioning that, as result of the research work of this Master program, the next two publications are being prepared (see Appendix A for details):

1. *Theta Method Applied to Two-Energy Groups Point Kinetics Equations.*
2. *Stochastic Point Reactor Kinetics Equations with Two-Energy Groups.*

Keywords: *nuclear reactor, stochastic Point Kinetics equations, neutron population, reactivity perturbation, temperature feedback*

CONTENTS

LIST OF TABLES

LIST OF FIGURES

LIST OF SYMBOLS

Symbol	Description
B^2	Buckling
C_i	Concentration of the i-th delayed neutron precursor group
D	Diffusion coefficient
E	Energy
g	Number of energy groups
G	Diffusion tensor
k_{eff}	Effective multiplication factor
K	Reciprocal of the thermal capacity of the reactor
m	Number of delayed neutron groups
N	Neutron density
q	Intensity of neutron source
Q	Neutron source
t	Time
T	Temperature
v	Speed of neutrons
V	Volume
W	Wiener process
α_T	Temperature coefficient of reactivity
β_i	Fraction of the i-th precursor group
γ^{-1}	Mean time for heat transfer to coolant
λ_i	Decay constant of the i-th precursor group
Λ	Mean generation time
ν	Mean number of neutrons born per fission event
ρ	Reactivity
Σ	Macroscopic Cross-Section

Subscripts

Cross sections	a	absorption
	f	fission
	s	scattering
	t	total remove
Two-Energy equations	1	Fast neutron group
	2	Thermal neutron group
Temperature	c	coolant
	r	reactor
Buckling	g	geometric
	m	material

1. INTRODUCTION

Energy production is a significant factor in the economic growth of countries [1, 2] and, if accompanied by adequate policies, it can improve the citizens life quality, especially in developing countries [3, 4]. Within the worldwide policies adopted to mitigate the emission of greenhouse gases, nuclear energy has been considered an ally of renewable energies [5, 6]. Thus, it is a task of the scientific community to know in-depth this physical system by means of, for instance, mathematical models and computer simulations, which allows to understand the behavior of the nuclear reactor under different scenarios, and reduce possible risks and increase safety.

The central problem in nuclear reactor theory is determining the neutron population into the reactor at each time. Usually, the focus is on two fundamental aspects involved in predicting the neutron population within the nuclear reactor, namely: *a*) determining the probabilities of the neutron-nucleus reactions; and, once these probabilities are known, *b*) deriving and solving an equation that uses these probabilities to determine the neutron population mechanisms in which neutrons can be gained or lost within an arbitrary volume. The result of this methodology is the neutron transport equation, which describes the evolution of the neutron current flux into the volume and its time evolution [7, 8]. As general aspects, the neutron population presents 7 degrees of freedom: 3 of them associated to space position, 2 for the angular dependence, 1 for energy, and 1 for time. However, it is usual to consider space isotropy, which allows to avoid treatment of the angular components to simplify the mathematical issue. Meanwhile, energy, as a continuous variable, is discretized into energy-groups due to the non-existence of an analytical expression for the neutron-nucleus interaction probabilities, as pointed out in several reports [9, 10, 11]. Moreover, the neutron transport equation exhibits non-linearity and stiffness[1]. For this reasons, analytical solutions are unknown, and, therefore, the numerical analysis represents an important tool in nuclear reactor theory.

This study is focused on homogeneous nuclear reactors, whose homogeneous connotation lays in the existent mixture of the fuel material with the moderator, and, in some cases, with the coolant material. The latter corresponding to liquid core reactors. A particular case of liquid core reactors is the Molten Salt Reactor (MSR), which is under extensive study due to its multiple advantages [12, 13, 14, 15]. On the other side, a simplified model that describes the dynamics of a homogeneous reactor is the Point Kinetics equations, proposed in the seminal work of Henry [16], which is valid for stationary fuel conditions, that is, when the isotopic

[1]The *stiffness* of a system of differential equations indicates that the solution can dramatically vary for small changes of the input parameters, causing instability in the numerical methods, i.e., no convergence of the numerical approximation to the solution. *Stiffness* may also occur when the variables evolve at very different times.

composition of the fuel is approximately constant while consumed due to the fission processes. Conversely, in general terms, the fuel isotopic composition gets modified when consumed. This effect is known as burn up [17].

The Point Kinetics equations model determines the time evolution of the neutron population in a homogeneous reactor with finite dimensions, as detailed in the works [7, 8], where the neutron shape population is time-independent and the neutron shape population is similar to that at the critical state. This condition is fulfilled for reactivity insertion rates up to 100% per second [16, 7]. This model is deterministic and can only estimate the mean values of the neutron population. Contrarily, the neutron-nucleus events are probabilistic in nature, what generates random fluctuations that cannot be described by the Point Kinetics equations model. An example of the random behavior of the reactor occurs at low population levels, as in the startup or shutdown of the reactor. In these scenarios the random variations are evident and must be taken into account [18, 19, 20, 21, 22]. Therefore, a stochastic model of the nuclear reactor is more accurate in modeling the random behavior than a deterministic one [23, 17].

The first stochastic Point Kinetics equations model was presented in 2005 by Hayes and Allen [24], and it consists of a system of nonlinear stochastic differential equations strongly coupled with stiffness in matrix form, which describes the time evolution of random variables as the neutron density and the concentration of delayed neutron precursors in a homogeneous nuclear reactor. The results of this model are in good agreement with the experimental available data. However, in this model, mono-energetic neutrons are considered, which implies assuming that neutron-nucleus interactions do not dependent on the neutron energy, which is far from reality, since it is observed that neutrons with low energy do have higher probability of interaction than those with higher energies. The purpose of this research is to provide physical rigor to the Hayes and Allen stochastic model by extending it to multi-energy groups, with the biggest emphasis on the two-group approximation, which has been shown to be accurate [25, 26, 27].

The stochastic Point Kinetics equations model with multi-energy groups and multi-groups of delayed neutrons[2] is derived in detail in Chap. 2, the numerical method proposed to solve it is described in Chap. 3. While Chap. 4 presents the results and discussions related to the proposed methodology when applied to two thermal homogeneous reactors. Finally, Chap. 5 summarizes our concluding remarks.

[2]Neutrons receive different names according to the time they appear inside the reactor. Thus, the apparition time of the neutrons born by fission (so-called prompt neutrons) is around 10^{-14} seconds, while delayed neutrons appear within 0.01 and 55 seconds. These neutrons are created as fission fragments, or from radioactive decay of atomic nuclei. Besides, since the range of time apparition is wide, the delayed neutrons are grouped according to the delay time, or, equivalently, to the decay constant of the precursor nucleus.

2. MODEL FORMULATION

In the following, we will derive the stochastic Point Kinetics equations model with two-energy groups and multi-groups of delayed neutrons. Initially, we will define the neutron density inside the reactor, to later derive the neutron diffusion equation from the neutron-nucleus interactions. Then, we will focus on the study of the time evolution of the neutron population. Further information, from basic concepts to more complex subjects beyond what is reported in this document can be accessed from the following sources [28, 7, 8].
Let us consider the number of neutrons within an arbitrary volume V with energies in the range $E \pm dE$, defined as

$$\left[\int_V N\left(\vec{r}, E, t\right) d^3r\right] dE, \tag{2.1}$$

where $N\left(\vec{r}, E, t\right)$ is the neutron density. The change in the number of neutrons in this volume is determined by various mechanisms such as those shown in **Fig. 2.1**[1,2].

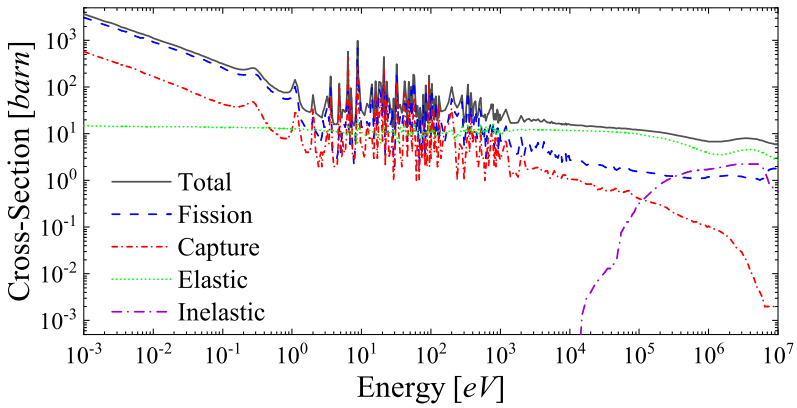

Figure 2.1: Energy dependence of the microscopic cross-section of ^{235}U.

Here, we observe the probability of occurrence of the different types of interactions between a neutron and a ^{235}U nucleus as a function on energy. This allows evidencing what was mentioned in the previous chapter, this is, neutrons with lower energies are more likely to interact than those with higher energies, except for the case of inelastic collisions.

[1]Data for this figure have been taken from the ENDF database [29].

[2]The *Cross-Section* stands for the probability that a specific neutron-nucleus reaction takes place. Let us consider a neutron beam impacting a target whose width is sufficiently thin (around one atomic layer thick) not to obtain shielding effect. One can expect the reaction rate to be proportional to both the beam intensity and the target area. Then, the proportionality constant is the reaction probability, which is called cross-section, and is expressed in area units. Thus, since the nuclear radius is roughly 10^{-12} cm, the cross-sectional area of a nucleus is roughly 10^{-24} cm^2, commonly called barns.

The equation:

$$\left[\int_V \frac{\partial}{\partial t} N\left(\vec{r}, E, t\right) d^3r\right] dE = gain\ in\ V\ -\ loss\ from\ V \tag{2.2}$$

describes the change in the neutron population.
The mechanisms that can lead to neutron appearances or disappearances in the V volume are as follows:

GAIN MECHANISM
I. Any neutron source within V.
II. Neutrons streaming into V through the surface S.
III. Neutrons suffering scattering collisions within V, which changes their energy from $E^{'}$ to E.

LOSS MECHANISM
IV. Neutrons leaking out through the surface S.
V. Neutrons suffering collisions within V causing absorption/removal of neutrons out of V, and scatterings moving the neutron energy from E to $E^{'}$.

According to this, Eqn.(2.2) can be rewritten as:

$$\left[\int_V \frac{\partial}{\partial t} N\left(\vec{r}, E, t\right) d^3r\right] dE = I\ +\ II\ +\ III\ -\ IV\ -\ V. \tag{2.3}$$

The mathematical expressions for each mechanism are defined below, starting from the simplest to the most difficult.

I. Source term: The rate of neutrons appearing in a volume d^3r centered at $\vec{r}$, within an energy range dE centered at E, is defined as $S\left(\vec{r}, E, t\right) d^3r dE$. Then, the number of neutrons appearing into V due to a source is:

$$I = \left[\int_V S\left(\vec{r}, E, t\right) d^3r\right] dE. \tag{2.4}$$

V. Loss due to collisions: The rate at which neutrons suffer collisions at a point $\vec{r}$ is $\vec{v}\left(E\right)$ $\Sigma_t\left(\vec{r}, E, t\right) N\left(\vec{r}, E, t\right)$, where $\vec{v}\left(E\right)$ stands for the neutron velocity and $\Sigma_t\left(\vec{r}, E, t\right)$ is the total remove cross-section. This cross-section includes all the neutron-nucleus events that remove neutrons such as inelastic scatterings, absorptions such as fission or radioactive capture (neutron-alpha, beta, gamma ray) events. Thus, the number of neutrons disappearing from V due to collisions is given by:

$$V = \left[\int_V \vec{v}\left(E\right) \Sigma_t\left(\vec{r}, E, t\right) N\left(\vec{r}, E, t\right) d^3r\right] dE. \tag{2.5}$$

III. Gains due to scatterings: The rate at which neutrons are scattered into the energy range dE centered at E coming from other energies $E^{'}$ is:

$$\int_0^\infty \vec{v}\left(E^{'}\right) \Sigma_s\left(\vec{r}, E^{'} \rightarrow E, t\right) N\left(\vec{r}, E^{'}, t\right) dE^{'}, \tag{2.6}$$

where $\Sigma_s\left(\vec{r}, E^{'} \rightarrow E, t\right)$ is the scattering cross-section. The number of neutrons appearing in V within the energy range dE centered at E is then:

$$III = \left[\int_V \int_0^\infty \vec{v}\left(E^{'}\right) \Sigma_s\left(\vec{r}, E^{'} \rightarrow E, t\right) N\left(\vec{r}, E^{'}, t\right) dE^{'} d^3r\right] dE. \tag{2.7}$$

This expression is known as the *in-scattering* term, since it characterizes the neutrons scattered from other energies into dE.

II and IV. Leakage into or from the volume: Combining these terms defines the net leakage through the surface S (see **Fig. 2.2**). Then, the rate at which neutrons leakage the volume through a piece of surface is $\vec{J}(\vec{r},E,t)\cdot d\vec{S}$, where $\vec{J}(\vec{r},E,t)$ is the neutron current density, defined as $\hat{n}\vec{v}(E)\,N(\vec{r},E,t)$. Therefore, the number of neutrons that leakage into or from the volume through the whole surface is given by:

$$II - IV = \oint_S \vec{J}(\vec{r},E,t)\cdot d\vec{S}dE = \int_V \vec{\nabla}\cdot\vec{J}(\vec{r},E,t)\,d^3rdE. \tag{2.8}$$

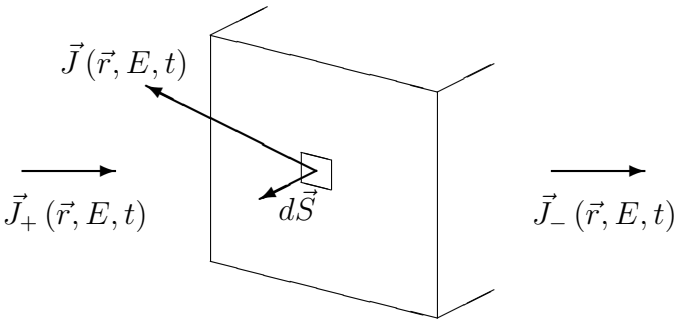

Figure 2.2: Schematic view of the net ($\vec{J}$) and partial contributions ($\vec{J}_-$ and $\vec{J}_+$) to the neutron current density.

The Divergence theorem is used in Eqn.(2.8) to have all the expressions in terms of volume integrals. Now that all the mechanisms that modify the number of neutrons within the volume have been described, Eqn.(2.3) reads as:

$$\int_V \left[\frac{\partial}{\partial t}N(\vec{r},E,t) + \vec{\nabla}\cdot\vec{J}(\vec{r},E,t) + \vec{v}(E)\,\Sigma_t(\vec{r},E,t)\,N(\vec{r},E,t) - \int_0^\infty \vec{v}\left(E'\right)\Sigma_s\left(\vec{r},E'\to E,t\right)N\left(\vec{r},E',t\right)dE' - S(\vec{r},E,t)\right]d^3r\;dE = 0. \tag{2.9}$$

Since the expression inside the square brackets cannot take negative values, this equation can be written as:

$$\frac{\partial}{\partial t}N(\vec{r},E,t) + \vec{\nabla}\cdot\vec{J}(\vec{r},E,t) + \vec{v}(E)\,\Sigma_t(\vec{r},E,t)\,N(\vec{r},E,t) = \int_0^\infty \vec{v}\left(E'\right)\Sigma_s\left(\vec{r},E'\to E,t\right)N\left(\vec{r},E',t\right)dE' + S(\vec{r},E,t)\,. \tag{2.10}$$

In Eqn.(2.10) we find two unknown terms, the neutron density given by $N(\vec{r},E,t)$, and the neutron current density represented by $\vec{J}(\vec{r},E,t)$. Unfortunately, there is no an exact relationship for describing one in terms of the other one. However, due to the null electric charge of the neutrons, their interactions with the medium are small, and they travel relatively long distances (about 1 to 100 cm depending on the medium), therefore, they slowly move from

high to low concentration regions. The magnitude of the neutron current density turns out to be proportional to the concentration gradient. Thus, the neutron current density can be written as:

$$\vec{J}(\vec{r},E,t) \simeq -D(\vec{r},E,t)\,\vec{v}(E)\,\vec{\nabla}N(\vec{r},E,t)\,. \tag{2.11}$$

The precedent equation is known as the Fick's law [30]. Here, $D(\vec{r},E,t)$ is the so-called diffusion coefficient, which gives a macroscopic description of the system, and its definition in nuclear theory is given by $D(\vec{r},E,t) = [3\Sigma_t(\vec{r},E,t)]^{-1}$ [7][3]. Therefore, Eqn.(2.10) is now written as:

$$\frac{\partial}{\partial t}N(\vec{r},E,t) - \vec{\nabla}\cdot D(\vec{r},E,t)\,\vec{v}(E)\,\vec{\nabla}N(\vec{r},E,t) + \vec{v}(E)\,\Sigma_t(\vec{r},E,t)\,N(\vec{r},E,t) = \int_0^\infty \vec{v}\left(E'\right)\Sigma_s\left(\vec{r},E'\to E,t\right)N\left(\vec{r},E',t\right)dE' + S(\vec{r},E,t)\,. \tag{2.12}$$

Equation (2.12) is know as the neutron diffusion equation, which usually has the neutron flux as unknown variable, that is, $\vec{v}(E)\,N(\vec{r},E,t)$. This equation has the initial condition $N(\vec{r},E,0) = N_0(\vec{r},E)$, and the boundary condition $N(\vec{r}_s,E,t) = 0$. This indicates that neutrons do not cross the boundaries of the reactor volume. The neutron diffusion equation is a linear integro-differential equation for neutron density with 5 degrees of freedom: 3 space coordinates, energy and time.

So far, a multiplicative medium has not been considered, as it is the case of a nuclear reactor, where neutrons cause fission events in the fuel material, which generates new neutrons. **Figure 2.3** shows the process of a ^{235}U nucleus being fissioned by the impact of a neutron. As a result of this interaction, two light atomic nuclei and three neutrons are generated. These are called *prompt* neutrons, since its time of appearance is 10^{-14} sec. On the other side, the light nucleus ^{86}Br decays to ^{87}Kr in an excited state, which finally decays to ^{86}Kr by emitting a neutron (see Figure **2.3**). This type of neutrons is called *delayed* neutrons since they take between 10^{-2} and 10^{2} seconds to appear. Delayed neutrons represent less than 1% of the neutron population within the reactor. Due to their appearance time, they allow to control the nuclear reactor, since, with them, the system evolution time is of the order of 10^{-3} seconds, while the evolution time would be about 10^{-6} seconds in their absence. For this reason, the delayed neutrons, despite representing a small part of the neutrons in the reactor, play a key role in the reactor safety. Moreover, let us note that prompt neutrons can generate new fissions, which, in turn, generate progressively more fission reactions. This mechanism is called a fission chain reaction. **Figure 2.3** also shows a radioactive capture event, a ^{235}U nucleus absorbs a neutron and emits gamma-rays.

Then, to include neutrons generated by fission events, the rate at which neutrons with any energy E' induce fission is defined as $\Sigma_f\left(\vec{r},E',t\right)\vec{v}\left(E'\right)N\left(\vec{r},E',t\right)$, where $\Sigma_f\left(\vec{r},E',t\right)$ is the fission cross-section. Therefore, the total rate at which prompt neutrons per fission event are born is given by:

[3] J. J. Duderstadt and L. J. Hamilton. (1976), p. 136 (Eqn. 4-147).

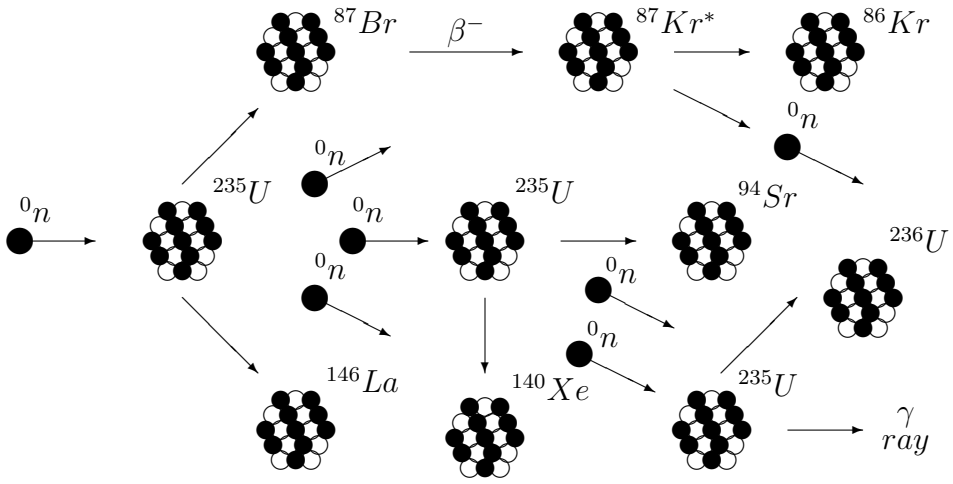

Figure 2.3: Schematic view of several neutron-nucleus interactions.

$$\int_0^\infty \chi^p\left(E'\right)(1-\beta)\,\nu\left(E'\right)\Sigma_f\left(\vec{r},E',t\right)v\left(E'\right)N\left(\vec{r},E',t\right)dE', \tag{2.13}$$

where, β is the fraction of delayed neutrons, $\nu\left(E'\right)$ is the average number of neutrons released per fission event, and $\chi^p\left(E'\right)$ is the fission spectrum, accounting for the energy distribution which the prompt neutrons are born with.

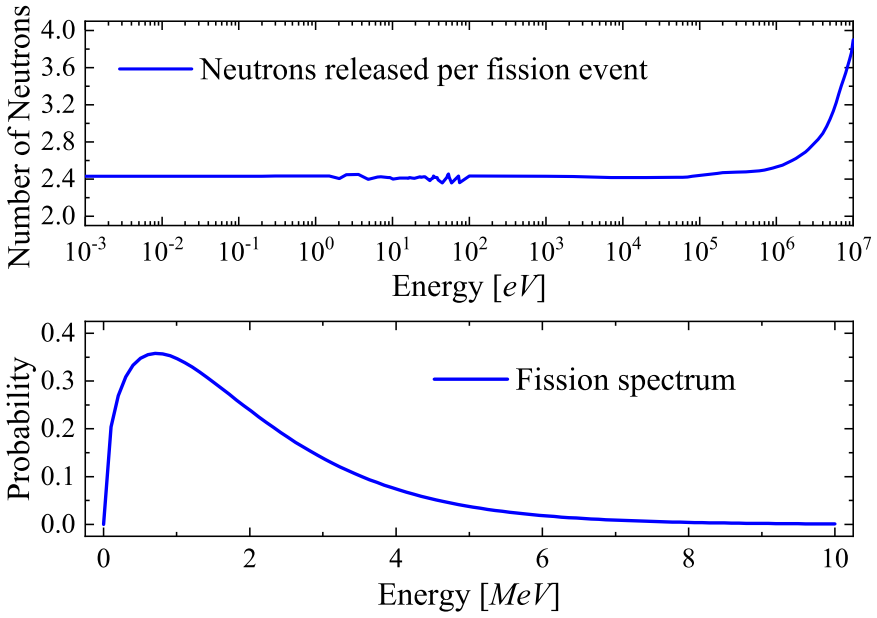

Figure 2.4: Mean number of neutrons released per fission event with thermal neutrons for ^{235}U (up), and neutron fission spectrum ($\chi^p(E)$) of the same isotope (bottom).

An empirical expression for this distribution is $\chi^p(E) = 0.453\sinh\left(\sqrt{2.29E}\right)e^{1.036E}$, which exhibits a bell-like behavior with a maximum located at around 0.7 MeV, and an average energy about 2 MeV [7][4]. **Figure 2.4**[5] shows the fission spectrum and the mean number of

[4] J. J. Duderstadt and L. J. Hamilton. (1976), p. 62 (Eqn. 2-112).

[5] Data for the mean number of neutrons released per fission event have been taken from the ENDF database [29] and the Duderstadt and Hamilton work [7] for the fission spectrum.

neutrons generated per fission event, which can be considered approximately constant, since, as mentioned above, neutrons with energies of the order of MeV have a low probability of generating fission.

Moreover, a wide variety of light atomic nuclei (which produce delayed neutrons) are generated by fission. These nuclei are usually classified accordingly to their half-life time (in the range 0.01 - 55 seconds). **Figure 2.5(a)**[6] shows the fission product yield as a function of the atomic mass. Usually, six groups of light nuclei are considered, as can be seen in **Table 2.1**[7], which reports the delayed neutron data for thermal fission of ^{235}U. However, in recent years a growing number of groups are being considered in the seek of accuracy [31]. **Figure 2.5(b)**[8] shows the energy spectra for delayed neutrons. It is observed that about 85% of the delayed neutrons born with energies between 0.1 and 1.4 MeV [33]. To include neutrons generated by radioactive decays, the rate at which delayed neutrons are born is then given by:

$$\chi^d(E)\sum_{i=1}^{m}\lambda_i C_i(\vec{r},t), \tag{2.14}$$

where $\chi^d(E)$ is the delayed neutron spectrum, λ_i is the decay constant of the i-group, and $C_i(\vec{r},t)$ is the concentration of delayed neutrons of the i-group.
Thus, the term for sources reads as:

$$S(\vec{r},E,t) = \int_0^{\infty}\chi^p\left(E'\right)(1-\beta)\,\nu\Sigma_f\left(\vec{r},E',t\right)\vec{v}\left(E'\right)N\left(\vec{r},E',t\right)dE' + \chi^d(E)\sum_{i=1}^{m}\lambda_i C_i(\vec{r},t) + q(\vec{r},E,t), \tag{2.15}$$

where $q(\vec{r},E,t)$ is an external source of neutrons. As example, some reactors use sticks of ^{252}Cf, which has a 3.1% probability of spontaneous fission, releasing 3.7 neutrons per fission event.

Table 2.1: Data for neutrons resulting from the thermal fission of ^{235}U. The groups (1 to 6) of delayed neutrons are explicitly reported according to their features such as half-life time, decay constant, energy, number of neutrons generated per fission event, and the relative fraction of neutrons inside the reactor.

Group	Half-Life [sec]	Decay constant [sec^{-1}]	Energy [MeV]	Neutrons per fission event	Fraction (β_i)
1	55.72	0.0124	0.250	0.00052	0.000215
2	22.72	0.0305	0.560	0.00346	0.001424
3	06.22	0.1110	0.405	0.00310	0.001274
4	02.30	0.3010	0.450	0.00624	0.002568
5	00.61	1.1400	-	0.00182	0.000748
6	00.23	3.0100	-	0.00066	0.000273
			Total neutrons per fission event:	0.01580	
				Total delayed fraction (β):	0.006502

[6]Data for this figure have been taken from the ENDF database [29].
[7]Data for this table have been taken from the Lamarsh and Baratta´s work [8]
[8]Data for the spectrum of delayed neutrons have been taken from the work [32].

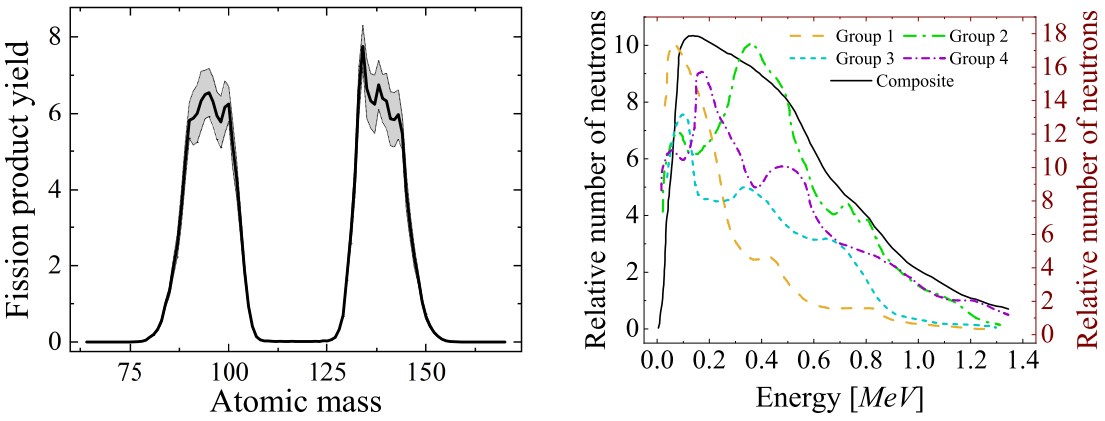

(a) Fission product yield. (b) Spectra of delayed neutrons.

Figure 2.5: Delayed neutron data: (a) Proportion of atomic nuclei generated by thermal neutron fission (shaded area represents the standard deviation); and (b) spectra of delayed neutrons selected by group and compound. Individual groups units are reported on the left axis (color curves); while the right axis is used for the composite signal (black curve).

After considering a multiplicative medium, such as the nuclear reactor, Eqn.(2.12) takes the form:

$$\frac{\partial}{\partial t}N\left(\vec{r},E,t\right)-\vec{\nabla}\cdot D\left(\vec{r},E,t\right)\vec{v}\left(E\right)\vec{\nabla}N\left(\vec{r},E,t\right)+\vec{v}\left(E\right)\Sigma_t\left(\vec{r},E,t\right)N\left(\vec{r},E,t\right)=$$
$$\int_0^\infty\left[\Sigma_s\left(\vec{r},E^{'}\rightarrow E,t\right)+\chi^p\left(E^{'}\right)\left(1-\beta\right)\nu\Sigma_f\left(\vec{r},E^{'},t\right)\right]\vec{v}\left(E^{'}\right)N\left(\vec{r},E^{'},t\right)dE^{'}$$
$$+\chi^d\left(E\right)\sum_{i=1}^{m}\lambda_i C_i\left(\vec{r},t\right)+q\left(\vec{r},E,t\right). \quad (2.16)$$

In the mathematical process, this equation is accompanied by the balance equation for delayed neutrons, which reads as:

$$\frac{\partial}{\partial t}C_i\left(\vec{r},t\right)=\int_0^\infty\beta_i\nu\Sigma_f\left(\vec{r},E^{'},t\right)\vec{v}\left(E^{'}\right)N\left(\vec{r},E^{'},t\right)dE^{'}-\lambda_i C_i\left(\vec{r},t\right), \quad (2.17)$$

where β_i is the fraction of delayed neutrons of the i-group, with i=1,2,...,m. And the initial condition is given by:

$$C_i\left(\vec{r},0\right)=\frac{\beta_i}{\lambda_i}\int_0^\infty\nu\Sigma_f\left(\vec{r},E^{'},t\right)\vec{v}\left(E^{'}\right)N\left(\vec{r},E^{'},t\right)dE^{'}. \quad (2.18)$$

Equations (2.16) and (2.17) describe the dynamics of a nuclear reactor. However, due to the lack of an analytical expression for the cross-sections, the energy spectrum of the neutrons is discretized into g-groups. Thus, the neutron density is redefined as:

$$N\left(\vec{r},E,t\right)=\sum_{g=1}^{G}N_g\left(\vec{r},t\right), \quad (2.19)$$

In addition, we consider time-independent cross-sections, which is valid for certain time intervals, and it is known as the stationary fuel condition. However, in broader scenarios, the

isotopic composition changes due to fission events, a process known as burn up, which modifies the neutron population distribution, and the stationary fuel condition is no longer valid [34]. Therefore, Eqns.(2.16) and (2.17) are written as:

$$\frac{\partial}{\partial t}N_g\left(\vec{r},t\right)-\vec{\nabla}\cdot D_g\left(\vec{r}\right)\vec{v}_g\vec{\nabla}N_g\left(\vec{r},t\right)+\vec{v}_g\Sigma_{g,t}\left(\vec{r}\right)N_g\left(\vec{r},t\right)= \sum_{g'=1}^{G}\left[\Sigma_s^{g'\rightarrow g}\left(\vec{r}\right)+\chi_{g'}^{p}\left(1-\beta\right)\nu\Sigma_{g',f}\left(\vec{r}\right)\right]\vec{v}_{g'}N_{g'}\left(\vec{r},t\right) + \chi_g^d\sum_{i=1}^{m}\lambda_i C_i\left(\vec{r},t\right)+q_g\left(\vec{r},t\right), \quad (2.20)$$

$$\frac{\partial}{\partial t}C_i\left(\vec{r},t\right)=\sum_{g'=1}^{G}\beta_i\nu\Sigma_{g',f}\left(\vec{r}\right)\vec{v}_{g'}N_{g'}\left(\vec{r},t\right)-\lambda_i C_i\left(\vec{r},t\right). \quad (2.21)$$

Remembering the strong relation of the neutron-nucleus interactions with neutron energy, the need to use a large number of energy groups could be assumed. Surprisingly, with few energy groups the description of the reactor is sufficiently accurate.

In this study, we focus on considering two-energy groups, which will be called **fast** and **thermal**. The fast group corresponds to neutrons with energies beyond 0.1 eV, and it is characterized by having less probability of generating fissions than the thermal group, which have energies around 0.025 eV.
Thus, once energies of the groups are determined, we have $\chi_1^p=\chi_1^d=1$ and $\chi_2^p=\chi_2^d=0$ since, on average, prompt neutrons are born with 2 MeV, and delayed neutrons are born with energies up to 0.1 MeV. Also, events of type $\Sigma_s^{1\rightarrow 2}$ are allowed, while the opposite are not. And, by definition, $\Sigma_{g,t}\left(\vec{r}\right)=\Sigma_{g,a}\left(\vec{r}\right)+\Sigma_s^{g\rightarrow g'}$, where $\Sigma_{g,a}$ is the absorption cross-section of g-group and $\Sigma_s^{g\rightarrow g'}$ is the scatter cross-section that removes neutrons off g towards g'-group. Then, $\Sigma_{1,t}\left(\vec{r}\right)=\Sigma_{1,a}\left(\vec{r}\right)+\Sigma_s^{1\rightarrow 2}$ and $\Sigma_{2,t}\left(\vec{r}\right)=\Sigma_{2,a}$. Therefore, Eqns.(2.20) and (2.21) become:

$$\frac{\partial}{\partial t}N_1\left(\vec{r},t\right)-\vec{\nabla}\cdot D_1\left(\vec{r}\right)\vec{v}_1\nabla N_1\left(\vec{r},t\right)+\vec{v}_1\Sigma_{1,t}\left(\vec{r}\right)N_1\left(\vec{r},t\right)= \left(1-\beta\right)\nu\left[\Sigma_{1,f}\left(\vec{r}\right)\vec{v}_1N_1\left(\vec{r},t\right)+\Sigma_{2,f}\left(\vec{r}\right)\vec{v}_2N_2\left(\vec{r},t\right)\right] + \sum_{i=1}^{m}\lambda_i C_i\left(\vec{r},t\right)+q_1\left(\vec{r},t\right), \quad (2.22a)$$

$$\frac{\partial}{\partial t}N_2\left(\vec{r},t\right)-\vec{\nabla}\cdot D_2\left(\vec{r}\right)\vec{v}_2\vec{\nabla}N_2\left(\vec{r},t\right)+\vec{v}_2\Sigma_{2,a}\left(\vec{r}\right)N_2\left(\vec{r},t\right)= \Sigma_s^{1\rightarrow 2}\left(\vec{r}\right)\vec{v}_1N_1\left(\vec{r},t\right)+q_2\left(\vec{r},t\right), \quad (2.22b)$$

$$\frac{\partial}{\partial t}C_i\left(\vec{r},t\right)=\beta_i\nu\left[\Sigma_{1,f}\left(\vec{r}\right)\vec{v}_1N_1\left(\vec{r},t\right)+\Sigma_{2,f}\left(\vec{r}\right)\vec{v}_2N_2\left(\vec{r},t\right)\right]-\lambda_i C_i\left(\vec{r},t\right), \quad (2.23)$$

Equations (2.22a), (2.22b), and (2.23) are known as the multi-groups neutron diffusion equations with two-energy groups and multi-groups of delayed neutrons [9]. These Eqns. describe the distribution of fast and thermal neutrons in the reactor and their time evolution.

Since stationary fuel has been assumed, the neutron population shape is time-independent, and similar to that at the critical state. This shape depends on the geometry of the reactor. Some of these shapes can be seen in **Fig 2.6**.

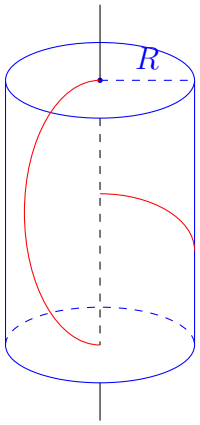

Cylinder of radius R and height H.

Shape: $\propto J_0\left(\frac{\alpha r}{R}\right) Cos\left(\frac{\pi z}{R}\right)$

Geometric buckling: $\left(\frac{\alpha}{R}\right)^2 + \left(\frac{\pi}{H}\right)^2$

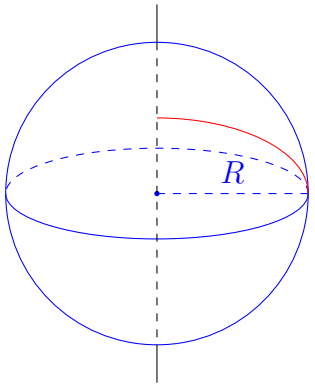

Sphere of radius R.

Shape: $\propto r^{-1} Sin\left(\frac{\pi r}{R}\right)$

Geometric buckling: $\left(\frac{\pi}{R}\right)^2$

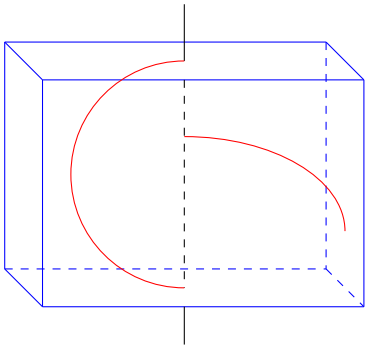

Rectangular parallelepiped with sides a, b, and c.

Shape: $\propto Cos\left(\frac{\pi x}{a}\right) Cos\left(\frac{\pi y}{b}\right) Cos\left(\frac{\pi z}{c}\right)$

Geometric buckling: $\left(\frac{\pi}{a}\right)^2 + \left(\frac{\pi}{b}\right)^2 + \left(\frac{\pi}{c}\right)^2$

Figure 2.6: Some sample geometries for nuclear reactors and the corresponding neutron shapes in red. Here, the term "neutron shape" represents the space distribution of the neutron population inside the reactor. For example, for cylindrical geometry, along the z-axis, shape is given by the Cosine function, while along the radial direction, it is given by Bessel functions. Curvature of these functions depends on the height and radius at the critical state of the reactor, respectively. Otherwise, curvature of the shape depends on the reactor elements.

Therefore, the main interest is the time evolution of the neutron population; and, given the statistical independence among the spatial and time variables, we can write:

$$N_g\left(\vec{r},t\right) = N_g\left(t\right)\Psi\left(\vec{r}\right), \quad C_i\left(\vec{r},t\right) = C_i\left(t\right)\Psi\left(\vec{r}\right), \quad and \quad q_g\left(\vec{r},t\right) = q_g\left(t\right)\Psi\left(\vec{r}\right), \tag{2.24}$$

where $\Psi\left(\vec{r}\right)$ is known as the Fundamental function and it determines the shape of the neutron population, for a given geometry.
This function is a solution to the equation $\nabla^2\Psi\left(\vec{r}\right) + B_{g,m}^2\Psi\left(\vec{r}\right) = 0$, where $B_{g,m}^2$ is the material buckling of the g-group, this parameter stands for the curvature of the shape (space distribution) adopted by the neutron population distribution inside the reactor. In general, the curvature of the space distribution of the neutron density depends on the reactor materials.

However, when the reactor is in a critical state, the curvature only depends on the reactor geometry, and it is known as geometrical buckling [7, 8]. Equations (2.22a), (2.22b), and (2.23) are then written as:

$$\frac{d}{dt}N_1(t) + D_1 v_1 B m_1^2 N_1(t) + v_1 \Sigma_{1,t} N_1(t) = (1-\beta)\,\nu\left[\Sigma_{1,f} v_1 N_1(t) + \Sigma_{2,f} v_2 N_2(t)\right] + \sum_{i=1}^{m} \lambda_i C_i(t) + q_1(t), \tag{2.25a}$$

$$\frac{d}{dt}N_2(t) + D_2 v_2 B m_2^2 N_2(t) + v_2 \Sigma_{2,a} N_2(t) = \Sigma_s^{1\to 2} v_1 N_1(t) + q_2(t), \tag{2.25b}$$

$$\frac{d}{dt}C_i(t) = \beta_i \nu\left[\Sigma_{1,f} v_1 N_1(t) + \Sigma_{2,f} v_2 N_2(t)\right] - \lambda_i C_i(t). \tag{2.26}$$

However, we must determine the material buckling. To do it, let us consider Eqns. (2.25a) and (2.25b) at the critical state; this is, when the number of neutrons produced by fission events and scatterings equals the number of lost neutrons by absorption mechanisms and scattering. This is:

$$D_1 v_1 B m_1^2 N_1(t) + v_1 \Sigma_{1,t} N_1(t) = \nu k_{\text{eff}}^{-1}\left[\Sigma_{1,f} v_1 N_1(t) + \Sigma_{2,f} v_2 N_2(t)\right], \tag{2.27a}$$

$$D_2 v_2 B m_2^2 N_2(t) + v_2 \Sigma_{2,a} N_2(t) = \Sigma_s^{1\to 2} v_1 N_1(t). \tag{2.27b}$$

From these expressions we obtain:

$$B m_1^2 = \frac{\nu k_{\text{eff}}^{-1}\left[\Sigma_{1,f} v_1 N_1(t) + \Sigma_{2,f} v_2 N_2(t)\right]}{D_1 v_1 N_1(t)} - \frac{\Sigma_{1,t}}{D_1}; \tag{2.28a}$$

$$B m_2^2 = \frac{\Sigma_s^{1\to 2} v_1 N_1(t)}{D_2 v_2 N_2(t)} - \frac{\Sigma_{2,a}}{D_2}, \tag{2.28b}$$

where, k_{eff}^{-1} is a parameter introduced to fit the behavior of the neutron population due to the use of cross-sections that can be inaccurate in some extent. Therefore, if $k_{\text{eff}}^{-1} = 1$ fails to predict the critical state, the k_{eff}^{-1} value can be fitted to obtain a stationary solution indicating the critical state of the reactor. The so-adjusted value of k_{eff}^{-1} is then used to predict the time evolution of the reactor out of a critical state [16]. It is also used to determine a critical size and composition of the nuclear reactor [7]. Then, hereafter the fission cross-section will be accompanied by the k_{eff}^{-1} parameter.

Let us define the following parameters, (ρ_g) *reactivity*, which measures the deviation from the critical state of the reactor. It can be understood as the difference between 1 and the ratio between the number of neutrons lost due to absorption and scattering events and the number of neutrons generated by fission events:

$$\rho_g = 1 - \left(\Sigma_{g,a} + D_g B m_g^2\right)\left(k_{\text{eff}}^{-1}\nu\Sigma_{g,f}\right)^{-1}. \tag{2.29}$$

Note that whenever a reactor is supercritical (this is, the number of neutrons that are born by fission events exceeds the deaths due to absorption and scattering) the condition $(\Sigma_{g,a} + D_g B m_g^2)\left(k_{\text{eff}}^{-1}\nu\Sigma_{g,f}\right)^{-1} < 1$ is fulfilled, and, in consequence, ρ_g is positive.

Conversely, in a subcritical reactor, the condition $\left(\Sigma_{g,a} + D_g B m_g^2\right)\left(k_{\text{eff}}^{-1}\nu\Sigma_{g,f}\right)^{-1} > 1$ holds, and ρ_g is negative.

Finally, $\rho_g = 0$ is the special case of a critical reactor, where the number of neutron births equals deaths. Thus, ρ_g values are restricted to the range $-\infty < \rho_g < 1$ [8].

Let Λ_g be the *Mean neutron generation time*, which measures the time a neutron takes from its birth up to it is absorbed:

$$\Lambda_g = \left(v_g k_{\text{eff}}^{-1} \nu \Sigma_{g,f}\right)^{-1} \tag{2.30}$$

These quantities are introduced due to the high difficulty of measuring the cross-sections when the reactor is in operation. Adopting these definitions, Eqns. (2.25a), (2.25b), and (2.26) are written as:

$$\begin{aligned} \frac{d}{dt}N_1(t) = &-\frac{1-\rho_1-\alpha}{\Lambda_1}N_1(t) - \kappa N_1(t) \longrightarrow \text{Deaths} \\ &+ \frac{1-\beta-\alpha}{\Lambda_1}N_1(t) + \frac{1-\beta}{\Lambda_2}N_2(t) \longrightarrow \text{Births} \\ &+ \sum_{i=1}^{m}\lambda_i C_i(t) \longrightarrow \text{Transformations} \\ &+ q_1(t) \longrightarrow \text{External Source}, \end{aligned} \tag{2.31a}$$

$$\begin{aligned} \frac{d}{dt}N_2(t) = &-\frac{1-\rho_2-\alpha}{\Lambda_2}N_2(t) \longrightarrow \text{Deaths} \\ &- \frac{\alpha}{\Lambda_2}N_2(t) + \kappa N_1(t) \longrightarrow \text{Births} \\ &+ q_2(t) \longrightarrow \text{External Source}, \end{aligned} \tag{2.31b}$$

$$\begin{aligned} \frac{d}{dt}C_i(t) = &\mu_{i,1}N_1(t) + \mu_{i,2}N_2(t) \longrightarrow \text{Births} \\ &- \lambda_i C_i(t) \longrightarrow \text{Deaths}, \end{aligned} \tag{2.32}$$

where $\alpha = \nu^{-1}$, $\mu_{i,g} = \beta_i \Lambda_g^{-1}$, and $\kappa = v_1 \Sigma_s^{1\to 2}$.

Equations (2.31a), (2.31b), and (2.32) are the deterministic Point Kinetics model with two-energy groups and multi-groups of delayed neutrons, which was presented in 2012 by A. A. Nahla in his seminal work [35] using the one-group of delayed neutron approximation. Additionally, in each equation, we have labeled the terms corresponding to the events of deaths, births, external sources, and radioactive decays, which will be useful for the derivation of the stochastic model.

To derive the stochastic Point Kinetics equations model with two-energy groups and multi-groups of delayed neutrons, let us define a new group of terms, namely: the neutron deaths rate due to capture and leakage for the g-group represented by $d_g = (1-\rho_g-\alpha)\Lambda_g^{-1}$; the neutron births rate due to fission for the g-group given by $b_g = \alpha\Lambda_g^{-1}$; the neutron births rate due to external sources for the g-group named q_g; the rate of births in the fast group due to radioactive decays of precursors i-group called $\lambda_i c_i$; and finally, the rate of neutrons that lose energy by collisions, going from fast to thermal groups represented by κ. Thus, the total number of events that change the populations (neutrons and precursors) are $3G+(G-1)+m$. Now, let us consider the change vector in the populations defined as

$$\Delta\vec{X} = \begin{bmatrix}\Delta n_1 & \Delta n_2 & \Delta c_1 & \Delta c_2 & \dots & \Delta c_m\end{bmatrix}_{m+2,1}^{T}, \tag{2.33}$$

where the random variables n_k and c_k are the number of neutrons and delayed neutron precursors, respectively. Conversely to Hayes and Allen, who use density as variable, we have chosen the random variables as the population number since, as we will see below, the quantities involved in describing the population changes come from individual neutron-nucleus interactions and not from density changes in a unit volume. However, the chosen random variables remain continuous because the cross-sections are average values of the neutron-nucleus interactions. Let us consider a small time interval Δt, where the occurrence probability of more than one event is zero, thus, the mathematical expressions for the $3G + (G-1) + m$ events changing the neutron population are defined as:

Deaths:

$\Delta\vec{X}_1 = \begin{bmatrix}-1 & 0 & 0 & 0 & ... & 0\end{bmatrix}^T_{m+2,1}$ $\longrightarrow$ A fast neutron dies due to capture or leakage with probability $P_1 = d_1 n_1 \Delta t$,

$\Delta\vec{X}_2 = \begin{bmatrix}0 & -1 & 0 & 0 & ... & 0\end{bmatrix}^T_{m+2,1}$ $\longrightarrow$ A thermal neutron dies due to capture or leakage with probability $P_2 = d_2 n_2 \Delta t$,

External Sources:

$\Delta\vec{X}_3 = \begin{bmatrix}1 & 0 & 0 & 0 & ... & 0\end{bmatrix}^T_{m+2,1}$ $\longrightarrow$ A fast neutron is born due to external source with probability $P_3 = q_1 \Delta t$,

$\Delta\vec{X}_4 = \begin{bmatrix}0 & 1 & 0 & 0 & ... & 0\end{bmatrix}^T_{m+2,1}$ $\longrightarrow$ A thermal neutron is born due to external source with probability $P_4 = q_2 \Delta t$,

Radioactive Decays:

$\Delta\vec{X}_5 = \begin{bmatrix}1 & 0 & -1 & 0 & ... & 0\end{bmatrix}^T_{m+2,1}$ $\longrightarrow$ A precursor of the first group decays by emitting a fast neutron with probability $P_5 = \lambda_1 c_1 \Delta t$,

$\vdots$

$\Delta\vec{X}_{m+4} = \begin{bmatrix}1 & 0 & 0 & 0 & ... & -1\end{bmatrix}^T_{m+2,1}$ $\longrightarrow$ A precursor of the m group decays by emitting a fast neutron with probability $P_{m+4} = \lambda_m c_m \Delta t$,

Scattering:

$\Delta\vec{X}_{m+5} = \begin{bmatrix}-1 & 1 & 0 & 0 & ... & 0\end{bmatrix}^T_{m+2,1}$ $\longrightarrow$ A fast neutron suffers collisions losing energy and reaches the thermal group with probability $P_{m+5} = \kappa n_1 \Delta t$,

Fissions:

$\Delta\vec{X}_{m+6} = \begin{bmatrix}\zeta_1 & 0 & \beta_1\nu & \beta_2\nu & ... & \beta_m\nu\end{bmatrix}^T_{m+2,1}$ $\longrightarrow$ A fast neutron generates fission, then a neutron dies, and $(1-\beta)\nu$ neutrons are generated, also precursor groups are generated with probability $P_{m+6} = b_1 n_1 \Delta t$,

$\Delta\vec{X}_{m+7} = \begin{bmatrix}\zeta_2 & -1 & \beta_1\nu & \beta_2\nu & ... & \beta_m\nu\end{bmatrix}^T_{m+2,1}$ $\longrightarrow$ A thermal neutron generates fission, then a neutron dies, and $(1-\beta)\nu$ fast neutrons are generated, also precursor groups are generated with probability $P_{m+7} = b_2 n_2 \Delta t$,

where $\zeta_1 = -1 + (1-\beta)\nu$ and $\zeta_2 = \zeta_1 + 1$.

Finally, the event corresponding to no changes in the population is included below, this event is important since it is used to obtain a normalized probability.

$$\Delta\vec{X}_{m+8} = \begin{bmatrix} 0 & 0 & 0 & 0 & \dots & 0 \end{bmatrix}^T_{m+2,1} \longrightarrow \text{No changes in neutron populations with probability } P_{m+8} = 1 - \sum_{k=1}^{3G+(G-1)+m} P_k.$$

These events are independent and represent counts of the population, which varies at a constant time rate. Hereby, it is the sum of these variables what represents the evolution of the populations within the reactor. We use the Central Limit Theorem (CLT) in its Lindeberg–Lévy form, which establishes that the sequence of independent and identically distributed random variables approximates a Normal distribution with zero as mean and one as variance [36]. Thus, the Lindeberg–Lévy CLT form reads as:

$$\sqrt{\text{Var}\left[\Delta\vec{X}\right]}\,\vec{\aleph}\,(0,1) \simeq \sqrt{n_e}\left(\Delta\vec{X} - \text{E}\left[\Delta\vec{X}\right]\right), \tag{2.34}$$

where $\vec{\aleph}\,(0,1)$ is a vector whose components are normal distributions with mean 0 and variance 1; $\Delta\vec{X}$ is the sample mean; $\text{E}\left[\Delta\vec{X}\right]$ and $\text{Var}\left[\Delta\vec{X}\right]$ are the vector of mean values and the matrix of standard deviations of $\Delta\vec{X}$, respectively; and n_e is the number of events considered. This indicates that the random variable and its sequence (or sample path) of $\Delta\vec{X}$ are independent and identically distributed, thus being inhomogeneous Poisson processes [37, 38].

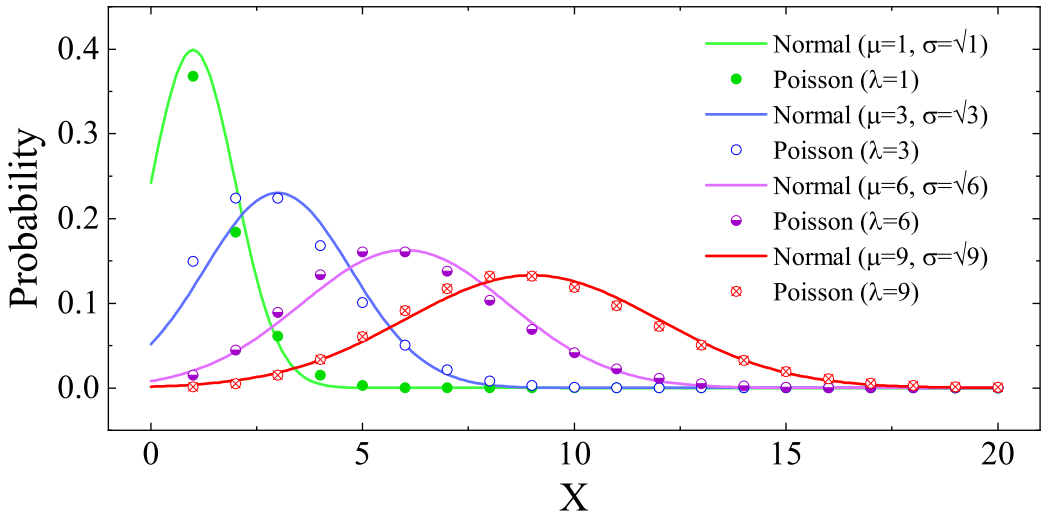

Figure 2.7: Schematic view of the Poisson and Normal distributions with different parameters.

This implies that the sample mean of a population is normally distributed regardless of the original distribution of the random variables. This can be clearly seen in **Fig. 2.7**, since the sum of Poisson distributions is a Poisson distribution whose parameter λ is the sum of the parameters of the distributions that make it up. The resulting distribution closely approximates a Normal one. Equation (2.34) is then written as:

$$\Delta\vec{X} = \text{E}\left[\Delta\vec{X}\right] + \frac{\sqrt{\text{Var}\left[\Delta\vec{X}\right]}\,\vec{\aleph}\,(0,1)}{\sqrt{n_e}}. \tag{2.35}$$

The mean value is computed as:

$$\begin{aligned}\mathrm{E}\left[\Delta\vec{X}\right] &= \sum_{k=1}^{3G+(G-1)+m} \Delta\vec{X}_k P_k \\ &= \Delta t \begin{bmatrix} \frac{\rho_1-\beta}{\Lambda_1} n_1(t) - \kappa n_1(t) + \frac{1-\beta}{\Lambda_2} n_2(t) + \sum_{i=1}^{m} \lambda_i c_i(t) + q_1(t) \\ \frac{\rho_2-1}{\Lambda_2} n_2(t) + \kappa n_1(t) + q_2(t) \\ \mu_{1,1} n_1(t) + \mu_{1,2} n_2(t) - \lambda_1 c_1(t) \\ \vdots \\ \mu_{m,1} n_1(t) + \mu_{m,2} n_2(t) - \lambda_m c_m(t) \end{bmatrix}_{m+2,1} \\ &= \left(A\vec{X} + \vec{Q}\right)\Delta t, \end{aligned} \tag{2.36}$$

where $\vec{X} = \begin{bmatrix} n_1(t) & n_2(t) & c_1(t) & c_2(t) & \dots & c_m(t) \end{bmatrix}^T_{m+2,1}$ is the vector of random variables; $\vec{Q} = \begin{bmatrix} q_1(t) & q_2(t) & 0 & \dots & 0 \end{bmatrix}^T_{m+2,1}$ is the vector of external sources; and A is a square matrix of dimension $(m+2)$ defined as:

$$A = \begin{bmatrix} a_{1,1} & a_{1,2} & \lambda_1 & \lambda_2 & \dots & \lambda_m \\ a_{2,1} & a_{2,2} & 0 & 0 & \dots & 0 \\ \mu_{1,1} & \mu_{1,2} & -\lambda_1 & 0 & \dots & 0 \\ \mu_{2,1} & \mu_{2,2} & 0 & -\lambda_2 & \dots & 0 \\ \vdots & \vdots & \vdots & \vdots & \ddots & \vdots \\ \mu_{m,1} & \mu_{m,2} & 0 & 0 & \dots & -\lambda_m \end{bmatrix}_{m+2,m+2}, \tag{2.37}$$

where $a_{1,1} = (\rho_1 - \beta - \Lambda_1\kappa)\Lambda_1^{-1}$; $a_{1,2} = (1-\beta)\Lambda_2^{-1}$; $a_{2,1} = \kappa$; and $a_{2,2} = (\rho_2 - 1)\Lambda_2^{-1}$.
The co-variance matrix is computed as:

$$\mathrm{Var}\left[\Delta\vec{X}\right] = \sum_{k=1}^{3G+(G-1)+m} \Delta\vec{X}_k \Delta\vec{X}_k^T P_k. \tag{2.38}$$

Nevertheless, this co-variance matrix can be replaced by the so-called Diffusion tensor due to the equivalence existing in the stochastic differential equation model [39]. This Diffusion tensor has been recently tested in the stochastic Point Kinetics equations model [40, 41] as well as in stochastic models of chemical reactions [42], with good agreement. Therefore, we now write:

$$\sqrt{\mathrm{Var}\left[\Delta\vec{X}\right]} = G\sqrt{\Delta t}, \tag{2.39}$$

where G (Diffusion tensor) is a rectangular $(m+2, 3G+(G-1)+m)$ matrix defined as:

$$G = \begin{bmatrix} \Delta\vec{X}_1\sqrt{P_1\Delta t^{-1}} & \dots & \Delta\vec{X}_{3G+(G-1)+m}\sqrt{P_{3G+(G-1)+m}\Delta t^{-1}} \end{bmatrix}_{m+2,3G+(G-1)+m}. \tag{2.40}$$

The columns of the Diffusion tensor are composed by the $\Delta\vec{X}_k$ vectors and their probabilities P_k. The main advantage of using the Diffusion tensor is that the computation of the square root of the co-variance matrix is not required, a process that is analytically non-trivial and computationally time-consuming.

The equivalence between the co-variance matrix and the Diffusion tensor can be proved by considering a N-dimensional stochastic processes $\vec{X}_t$, whose time evolution is given by:

$$d\vec{X}_t = \vec{\mu}\left(t, \vec{X}_t\right) dt + \sqrt{V\left(t, \vec{X}_t\right)} d\vec{W}_t, \tag{2.41}$$

where, $V\left(t, \vec{X}_t\right)$ is a square matrix of dimension $N \times N$. The time evolution of the probability density function $P\left(t, \vec{X}_t\right)$ is described by the Fokker-Planck relationship, also known as the forward Kolmogorov equation [43, 44, 45], which reads as:

$$\frac{\partial}{\partial t} P\left(t, \vec{X}_t\right) = -\sum_{i=1}^{N} \frac{\partial}{\partial x_i}\left[\mu_i P\left(t, \vec{X}_t\right)\right] + \sum_{i=1}^{N}\sum_{j=1}^{N} \frac{\partial^2}{\partial x_i \partial x_j}\left[V_{i,j} P\left(t, \vec{X}_t\right)\right]. \tag{2.42}$$

Now, let us consider the matrices $B\left(t, \vec{X}_t\right)$ and $G\left(t, \vec{X}_t\right)$, with dimensions $N \times N$ and $N \times M$, respectively. The relation between the $V\left(t, \vec{X}_t\right)$ matrix and the matrices $B\left(t, \vec{X}_t\right)$ and $G\left(t, \vec{X}_t\right)$ is given by:

$$B\left(t, \vec{X}_t\right) = \sqrt{V\left(t, \vec{X}_t\right)} \tag{2.43}$$

$$V\left(t, \vec{X}_t\right) = G\left(t, \vec{X}_t\right) G\left(t, \vec{X}_t\right)^T. \tag{2.44}$$

Note that the entries of the $V\left(t, \vec{X}_t\right)$ matrix can be written as: $V_{i,j} = \sum_{l=1}^{N} B_{i,l} B_{l,j}$ or $V_{i,j} = \sum_{l=1}^{M} G_{i,l} G_{l,j}$. Therefore, the stochastic process $\vec{X}_t$ can be described by:

$$d\vec{X}_t = \vec{\mu}\left(t, \vec{X}_t\right) dt + B\left(t, \vec{X}_t\right) d\vec{W}_t \tag{2.45}$$

$$d\vec{X}_t = \vec{\mu}\left(t, \vec{X}_t\right) dt + G\left(t, \vec{X}_t\right) d\vec{W}_t^*, \tag{2.46}$$

where $\vec{W}_t$ is a N-dimensional Wiener process and $\vec{W}_t^*$ is a M-dimensional Wiener process independent of the previous one. These equations lead to the same Fokker-Planck equation. Then, the evolution of the stochastic process $\vec{X}_t$ can be represented in two different forms. Consequently, does exist a Wiener process $\vec{W}$ that generates a sample path for $\vec{X}$ (process realization), and an independent Wiener process $\vec{W}^*$ that generates the same sample path. The equivalence of the stochastic differential equations is discussed in more detail in references [39, 46].

Taking into account Eqns. (2.36) and (2.39), Eqn. (2.35) is rewritten as:

$$\Delta\vec{X} = \left(A\vec{X} + \vec{Q}\right)\Delta t + \frac{1}{\sqrt{n_e}} G\sqrt{\Delta t}\vec{\aleph}(0,1). \tag{2.47}$$

Now, considering $\Delta t \longrightarrow 0$, the system of Itô stochastic differential equations in matrix form is obtained:

$$d\vec{X}_t = \left(A_t\vec{X}_t + \vec{Q}_t\right) dt + \frac{1}{\sqrt{n_e}} G_t d\vec{W}_t, \tag{2.48}$$

where $d\vec{W}_t$ is a vector of dimension $(3G + (G-1) + m, 1)$ defined as $\sqrt{dt}\vec{\aleph}(0,1)$, whose components W_k are independent Wiener processes (or Brownian movements) with independent

stationary increases. Its properties are: $W_k(t=0) = 0$ with probability 1; and $W_k(t) - W_k(s) = \aleph(0, t-s)$ for $0 \leq s < t \leq T$.
$\aleph(0, t-s)$ denotes the Normal distribution of expected value 0 and standard deviation $\sqrt{t-s}$; and the increments $W_k(t) - W_k(s)$ and $W_k(v) - W_k(u)$ are independent from each other for $0 \leq s < t < u < v \leq T$ [47].

Equation (2.48) is the stochastic Point Kinetics model with two-energy groups and multi-groups of delayed neutrons. Regretfully, it does not have analytical solution. Therefore, numerical techniques must be applied to get approximate solutions. Let us note that if $G = 0$, Eqn. (2.48) reduces to the deterministic model of Point Kinetics equations with two-energy groups [35]. Therefore, the stochastic model can be considered as a generalization of the deterministic model.

One additional key aspect must be addressed; in a nuclear reactor, the reactivity can change over time due to external mechanisms such as the insertion of control elements inside the reactor to regulate the neutron population, and to physical variations such as temperature changes caused by the energy released as result of fission events. Therefore, the reactivity (ρ) is written as a sum of an initial reactivity (ρ_0) plus a feedback reactivity:

$$\rho(t) = \rho_0(t) + \rho_f(t). \tag{2.49}$$

As it is well known, temperature variations modify the atomic density of the fuel, which changes in turn the values of the cross-sections. Therefore, changes in the reactivity due to this effect can be written in terms of the temperature reactivity coefficient α_T. Then, assuming an isothermal model where the reactor temperature is represented by an effective temperature T_r, the change in the feedback reactivity is:

$$\frac{\partial}{\partial T_r}\rho_f(t) = \alpha_T. \tag{2.50}$$

On the other hand, the heat produced in the reactor by the energy released in the fission events is extracted through a hydraulic circuit, which cools the reactor. A model for this heat exchange is given by the Newton's law of cooling:

$$\frac{d}{dt}T_r(t) = Kn(t) - \gamma\left(T_r(t) - T_c\right), \tag{2.51}$$

where T_c is the coolant temperature, K is the reciprocal of the thermal capacity of the reactor, and γ^{-1} is the mean time for heat transfer to coolant. Therefore, with this in mind, Eqn. (2.49) now takes the form:

$$\rho(t) = \rho(t_0) + \rho_0(t) + \alpha_T K \int_0^t n\left(t'\right) e^{-\gamma t'} dt'. \tag{2.52}$$

Equations (2.51) and (2.52) include the effects of temperature within the reactor.
Thus, the stochastic Point Kinetics equations model with two-energy groups and multi-groups of delayed neutrons is complete.

The next chapter discusses the numerical scheme proposed to provide numerical solutions to the derived model.

3. NUMERICAL APPROXIMATION

In the previous chapter, the stochastic Point Kinetics equations model with two-energy groups and multi-groups of delayed neutrons was deduced. As discussed, this model describes the time evolution of the neutron and precursors populations in a homogeneous nuclear reactor, and is represented by the Itô stochastic differential equation:

$$d\vec{X}_t = \left(A_t\vec{X}_t + \vec{Q}_t\right)dt + \frac{1}{\sqrt{n}}G_t d\vec{W}_t, \tag{3.1}$$

whose solution is:

$$\vec{X}_t - \vec{X}_{t_0} = \int_{t_0}^{t} a\left(t, \vec{X}_t\right)dt + \frac{1}{\sqrt{n}}\int_{t_0}^{t} G\left(t, \vec{X}_t\right)d\vec{W}_t, \tag{3.2}$$

where $a\left(t, \vec{X}_t\right) = A_t\vec{X}_t + \vec{Q}_t$.

It is well known that there is a trouble with the computation of the integral involving the Wiener process (W_t) since, strictly, it is not differentiable because it is composed of a white noise $\aleph(0,1)$ exhibiting unbounded variation [48]. Nevertheless, to solve our problem we will use the Itô's lemma, which is the stochastic counterpart of the Chain Rule in traditional calculus. Using this lemma the differential of a stochastic process can be obtained. For instance, let us consider the stochastic process represented by $X_t = f(x_t)$ that satisfies the stochastic differential equation $dX_t = \mu(t, x_t)\,dt + \sigma(t, x_t)\,dW_t$. According to the Itô's lemma, if $f(x_t)$ is a twice-differentiable scalar function one has [48][1]:

$$df(x_t) = \left[\mu(t, x_t)\frac{\partial}{\partial x}f(x_t) + \frac{\sigma(t, x_t)}{2}\frac{\partial^2}{\partial x^2}f(x_t)\right]dt + \sigma(t, x_t)\frac{\partial}{\partial x}f(x_t)\,dW_t. \tag{3.3}$$

By integrating from t_0 to t, we obtain:

$$f(x_t) - f(x_{t_0}) = \int_{t_0}^{t}\left[\mu(t, x_t)\frac{\partial}{\partial x}f(x_t) + \frac{\sigma(t, x_t)}{2}\frac{\partial^2}{\partial x^2}f(x_t)\right]dt + \int_{t_0}^{t}\sigma(t, x_t)\frac{\partial}{\partial x}f(x_t)\,dW_t, \tag{3.4}$$

with the operators L^0 and L^1 given by $L^0 = \mu(t, x_t)\frac{\partial}{\partial x} + \frac{\sigma(t,x_t)}{2}\frac{\partial^2}{\partial x^2}$ and $L^1 = \sigma(t, x_t)\frac{\partial}{\partial x}$. Thus, Eqn. (3.4) becomes:

$$f(x_t) - f(x_{t_0}) = \int_{t_0}^{t} L^0 f(x_t)\,dt + \int_{t_0}^{t} L^1 f(x_t)\,dW_t. \tag{3.5}$$

[1] P. E. Kloeden and E. Platen. (1992), p. 163 (Eqn. 1.12)

Now, let us consider $f(x_t) = a(t, x_t)$ and $f(x_t) = G(t, x_t)$ according to Eqn. (3.5), this is:

$$a(t, x_t) - a(t_0, x_{t_0}) = \int_{t_0}^{t} L^0 a(t, x_t)\, dt + \int_{t_0}^{t} L^1 a(t, x_t)\, dW_t, \tag{3.6}$$

$$G(t, x_t) - G(t_0, x_{t_0}) = \int_{t_0}^{t} L^0 G(t, x_t)\, dt + \int_{t_0}^{t} L^1 G(t, x_t)\, dW_t. \tag{3.7}$$

Thus, by using these expressions in Eqn. (3.2) we obtain:

$$\vec{X}_t - \vec{X}_{t_0} = a\left(t_0, \vec{X}_{t_0}\right) \int_{t_0}^{t} dt + G\left(t_0, \vec{X}_{t_0}\right) \int_{t_0}^{t} d\vec{W}_t + R, \tag{3.8}$$

where the remaining term R is given by:

$$R = \int_{t_0}^{t}\int_{t_0}^{\tau} L^0 a\left(\tau, \vec{X}_\tau\right) dt d\tau + \int_{t_0}^{t}\int_{t_0}^{\tau} L^1 a\left(\tau, \vec{X}_\tau\right) dt dW_\tau + \int_{t_0}^{t}\int_{t_0}^{\tau} L^0 G\left(\tau, \vec{X}_\tau\right) dW_t d\tau + \int_{t_0}^{t}\int_{t_0}^{\tau} L^1 G\left(\tau, \vec{X}_\tau\right) dW_t dW_\tau. \tag{3.9}$$

This previous procedure gives rise to the so-called Itô-Taylor Expansion [48]. Now, by truncating this expansion in the second term on the right side on Eqn. (3.8), and solving the trivial integrals, the following expression is obtained:

$$\vec{X}_t - \vec{X}_{t_0} = a\left(t_0, \vec{X}_{t_0}\right) \Delta t + \frac{1}{\sqrt{n}} G\left(t_0, \vec{X}_{t_0}\right) \Delta W_t, \tag{3.10}$$

where $\Delta t = t - t_0$ and $\Delta W = W_t - W_{t_0}$. Also, by writing Eqn. (3.10) as a sequence of k equidistant discrete steps we obtain:

$$\vec{X}_{t_{k+1}} = \vec{X}_{t_k} + a\left(t_k, \vec{X}_{t_k}\right) \Delta t + \frac{1}{\sqrt{n}} G\left(t_k, \vec{X}_{t_k}\right) \Delta W_k, \tag{3.11}$$

with $\Delta t = t_{k+1} - t_k$ and $\Delta W = W_{t_{k+1}} - W_{t_k}$.

Equation (3.11) represents the iterative Euler-Maruyama scheme, which can be considered as a generalization of the traditional Euler scheme, that can be recovered with $G = 0$.
Since the system of equations making up our model exhibits stiffness[2], along with non-linearity and a strong coupling of the random variables, it is convenient to use implicit schemes in the seeking of bigger stability [49]. Therefore, let us consider the transformation $a\left(t_k, \vec{X}_{t_k}\right) \longrightarrow a\left(t_{k+1}, \vec{X}_{t_{k+1}}\right)$, thus, Eqn. (3.11) becomes:

$$\vec{X}_{t_{k+1}} = \vec{X}_{t_k} + \left(A_{t_{k+1}} \vec{X}_{t_{k+1}} + \vec{Q}_{t_{k+1}}\right) \Delta t + \frac{1}{\sqrt{n}} G\left(\vec{X}_{t_k}\right) \Delta W_k. \tag{3.12}$$

This is the implicit version of the Euler-Maruyama scheme, which works well in approximating solutions of the Hayes and Allen model [50]. Since the solution X_{k+1} is on both sides of Eqn. (3.12), this is an implicit equation. This fact can be considered a disadvantage since it requires

[2]Stiffness indicates that the solution can vary drastically for small changes on the input parameters, which causes instability in the numerical methods, i.e., the numerical approximation does not converge to the solution. This may also occur when the variables evolve at very different times. It is worth noting that our model presents both of these aspects.

algebraic resources to get the solution, which, in some cases, is not trivial form the analytical viewpoint, and it is computationally time-consuming. Despite these difficulties, in our case, it is solved through the following steps:

$$\left(I - A_{t_{k+1}}\Delta t\right)\vec{X}_{t_{k+1}} = \vec{X}_{t_k} + \vec{Q}_{t_{k+1}}\Delta t + \frac{1}{\sqrt{n}}G\left(\vec{X}_{t_k}\right)\Delta W_k, \tag{3.13}$$

$$\vec{X}_{t_{k+1}} = \left(I - A_{t_{k+1}}\Delta t\right)^{-1}\left[\vec{X}_{t_k} + \vec{Q}_{t_{k+1}}\Delta t + \frac{1}{\sqrt{n}}G\left(\vec{X}_{t_k}\right)\Delta W_k\right], \tag{3.14}$$

$$\vec{X}_{t_{k+1}} = M^{-1}_{t_{k+1}}\left[\vec{X}_{t_k} + \vec{Q}_{t_{k+1}}\Delta t + \frac{1}{\sqrt{n}}G\left(\vec{X}_{t_k}\right)\Delta W_k\right], \tag{3.15}$$

where I is the identity matrix and $M = I - A_{t_{k+1}}\Delta t$.

Equation (3.15) is the numerical approximation to the solution to the stochastic Point Kinetics equations model with two-energy groups and multi-groups of delayed neutrons. Here, the M^{-1} matrix is computed analytically by using the relation $MM^{-1} = I$, avoiding a waste of computational time. To describe the elements of the M^{-1} matrix, the following parameters are introduced: $e_i = h\mu_{i,2}\theta\left(1 + h\lambda_i\right)^{-1}$, and $E_i = h\left(\mu_{i,1} + h\mu_{i,2}a_{2,1}\theta\right)\left(1 + h\lambda_i\right)^{-1}$, with $\theta = \left(1 - ha_{2,2}\right)^{-1}$.
Thus, the $M_{i,j}$ elements of the M^{-1} matrix are given by:

$$M_{1,1} = \left(1 - ha_{1,1} - h^2a_{1,2}a_{2,1}\theta - h\textstyle\sum_{i=1}^{m}\lambda_iE_i\right)^{-1},$$

$$M_{1,2} = \left(ha_{1,2}\theta + h\textstyle\sum_{i=1}^{m}\lambda_ie_i\right)M_{1,1}, \qquad M_{2,1} = ha_{2,1}\theta M_{1,1},$$

$$M_{2,2} = \theta\left(1 + ha_{2,1}M_{1,2}\right), \qquad M_{1,i+2} = h\lambda_i\left(1 + h\lambda_i\right)^{-1},$$

$$M_{2,i+2} = ha_{2,1}\theta M_{1,i+2}, \qquad M_{i+2,1} = E_iM_{1,1},$$

$$M_{i+2,2} = e_i + E_iM_{1,2}, \qquad M_{i+2,j+2} = E_iM_{1,j+2} + \left(1 + h\lambda_i\right)^{-1}\delta_{i,j},$$

where $\delta_{i,j}$ is the Kronecker's delta (i.e. $\delta_{i,j}$=1 for $i = j$, and $\delta_{i,j}$=0 for $i \neq j$).
Additionally, Eqn. (2.51) is discretized by using the Euler method to obtain:

$$T_{r,k+1} = T_{r,k} + \left[Kn_k - \gamma\left(T_k - T_c\right)\right]\Delta t, \tag{3.16}$$

while, the Trapezoidal Rule [51, 52] is employed in Eqn. (2.52), giving:

$$\rho_{k+1} = \rho_k + \rho_{0n} + \frac{\alpha_TK}{2}e^{-\frac{\gamma}{2}\left(t_{k+1}+t_k\right)}\left(n_{t_{k+1}} + n_{t_k}\right)\Delta t. \tag{3.17}$$

Equations (3.15), (3.16) and (3.17) give the numerical solution to the stochastic Point Kinetics model with two-energy groups and multi-groups of delayed neutrons. The results are presented and discussed in depth in the next chapter.

4. RESULTS

After defining the complete set of equations describing the method in the previous chapter, in this chapter we discuss several practical results. In particular, we address the simulations of two thermal nuclear reactors studied under the stochastic Point Kinetics equations model with two-energy groups (SPKE-2E) and multi-group of delayed neutrons. Approximate numerical solutions were obtained using the Implicit Euler-Maruyama Method (IEM). To generate the Wiener processes, the MATLAB[1] function *rng(seed,'twister')* was implemented, with *seed* equals to 2794[2]. The results were compared, regarding mean and standard deviation values, with literature reports.

4.1 BENCHMARK

The first thermal reactor is a benchmark presented in 1973 by Ferguson and Hansen [54], which is a homogeneous bare cube of side length 200 cm, whose parameters are reported in **Table 4.1**.

Ferguson and Hansen originally studied the time evolution of neutron populations for a negative step perturbation in the thermal group absorption cross-section ($\Delta\Sigma_{2,a}$) with a reactivity worth about 0.5 Dollars[3] (or 50 cents), considering one group of delayed neutrons (this single precursor group represents the m precursor groups, with an average decay constant). Later, other authors considered six groups of delayed neutrons, with both, positive and negative time-independent and time-dependent perturbations, keeping constant the quantity $\Delta\Sigma_{2,a} = 0.369 \times 10^{-4}\ cm^{-1}$.

In this study, we address the cases of step, ramp and sinusoidal insertions with positive and negative perturbations. In all cases, the interval for time evolution of the neutron population is $[0, 0.4]$ seconds, with no external sources and initial conditions given by: $n_1(0) = 2.228930 v_1^{-1}$, $n_2(0) = 0.816356 v_2^{-1}$, and $c_i(0) = [\mu_{i,1} n_1(0) + \mu_{i,2} n_2(0)]\, \lambda_i^{-1}$.

To obtain the mean and standard deviation values, 5000 realizations of the stochastic process

[1] Version R2020a [53].

[2] This number allows the same sequence of pseudo-random numbers to be generated, enabling other researchers to replicate the results presented.

[3] Reactivity is a dimensionless quantity to which some units have been defined. One of them is the *Dollar* (\$), this unit indicates the amount of reactivity necessary to obtain instantaneous criticality; that is, the instantaneous neutrons generate a fission chain reaction such that the neutron population in the reactor remains constant over time. By definition a *Dollar* is the ratio between the reactor reactivity (ρ) and the effective fraction of delayed neutrons (β_{eff}), the latter being the quantity that accounts for those delayed neutrons that achieve thermal energies.

were executed. The selected reference values were chosen according to the time step and the significant digits reported for the neutron population, that is, time step of 10^{-3} and 6 digits.

Table 4.1: Parameters of a bare, homogeneous reactor.

Parameter	Fast neutrons	Thermal neutrons	Delayed group i	λ_i $[s^{-1}]$	β_i $(\times 10^{-3})$
D $[cm^{-1}]$	1.3500000	1.0800000	1	0.0127	0.2432
$\Sigma_a[cm^{-1}]$	0.0013820	0.0054869	2	0.0317	1.7920
$\Sigma_f[cm^{-1}]$	0.0002420	0.0040800	3	0.1150	1.3824
$\Sigma_s[cm^{-1}]$	0.0023000	-	4	0.3110	2.0992
v $[cm/s]$	3.00×10^7	2.20×10^5	5	1.4000	0.6592
ν	2.41		6	3.8700	0.2240
k_{eff}	0.8952858		*average*	*0.0800*	

4.1.1 Step Reactivity

Now, we study a time-independent reactivity insertion through a constant perturbation in the thermal group absorption cross-section given by $\Delta\Sigma_{2,a} = \pm 0.369 \times 10^{-4}\ cm^{-1}$.

Tables 4.2 and **4.3** report on those results obtained for positive (i.e., $\Delta\Sigma_{2,a} < 0$) and negative (i.e., $\Delta\Sigma_{2,a} > 0$) step reactivity perturbations[4], respectively. Reference values for positive step reactivity with one and six groups of delayed neutrons and negative step reactivity with six groups of delayed neutrons have been taken from the work of Aboanber *et. al* [55], where the numerical solutions are obtained by the Analytical Technique (AT) for a point reactor whose neutron population time evolution is described by a set of fractional differential equations. Also, the reference values for a negative step reactivity with one group of delayed neutrons case have been taken from the work by Aboanber and Nahla [56], where the multigroup neutron diffusion model is studied and the numerical solutions are obtained through the Adaptative Matrix Formation scheme (AMF). In these scenarios, IEM (this work) yields accurate results with percentage errors below 1.5%. Errors close to this value are obtained for negative insertions, while for positive insertions the percentage errors are about 1.0%. This small difference illustrates an important behavior; this is, for decreasing populations, the random fluctuations are more noticeable due to the probabilistic nature of the physical system and its description by means of average values of the cross-sections. This can be seen in **Fig. 4.1**, where the mean values fluctuate randomly most noticeably for negative insertions around the reference curves, which were generated for $G = 0$, i.e., the deterministic Point Kinetics equations model with two-energy groups.

[4]A perturbation $\Sigma_a + \Delta\Sigma_a$, with $\Delta\Sigma_a < 0$, decreases the probability for neutrons to die into the reactor, which implies an increase in the neutron population. Therefore, $\Delta\Sigma_a < 0$ represents a positive step reactivity insertion. The opposite, $(\Delta\Sigma_a > 0)$ represents a negative step reactivity insertion. This kind of perturbation can be caused by the action of control elements, which are made of highly neutron-absorbing materials such as boron or graphite.

Table 4.2: Data for the fast and thermal neutron fluxes using one and six precursors groups for positive step reactivity.

	Method		Time [s] 0.00	0.05	0.10	0.15	0.20	0.30	0.40
One Precursor	**AT***	Fast	2.228930	3.071553	3.831159	4.517422	5.139029	6.218113	7.119829
		Thermal	0.816356	1.127324	1.407597	1.660800	1.890138	2.288234	2.620862
	This work	Fast	2.228930	3.099886	3.879171	4.561264	5.204636	6.301385	7.121845
			(NA)	*(1.233172)*	*(1.748910)*	*(2.177223)*	*(2.575173)*	*(3.140105)*	*(3.607919)*
		Thermal	0.816356	1.136695	1.426276	1.677383	1.916339	2.318258	2.620738
			(NA)	*(0.443425)*	*(0.636724)*	*(0.794905)*	*(0.941016)*	*(1.149493)*	*(1.320985)*
Six Precursors	**AT***	Fast	2.228930	3.072767	3.839954	4.544745	5.198982	6.393180	7.482373
		Thermal	0.816356	1.127753	1.410772	1.670733	1.912010	2.352329	2.753829
	This Work	Fast	2.228930	3.078874	3.831837	4.558713	5.199003	6.392617	7.512016
			(NA)	*(0.944672)*	*(1.374357)*	*(1.720823)*	*(2.056507)*	*(2.580410)*	*(3.092402)*
		Thermal	0.816356	1.129493	1.406940	1.675496	1.911623	2.352754	2.765349
			(NA)	*(0.339258)*	*(0.499949)*	*(0.629887)*	*(0.751137)*	*(0.945384)*	*(1.135050)*

*$\alpha = 1$

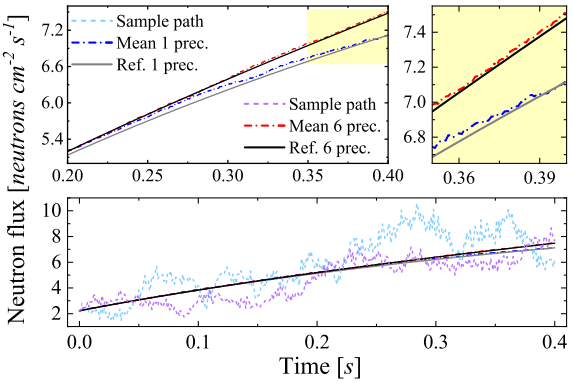

(a) Mean **fast** neutron fluxes and two sample paths for **positive** step reactivity.

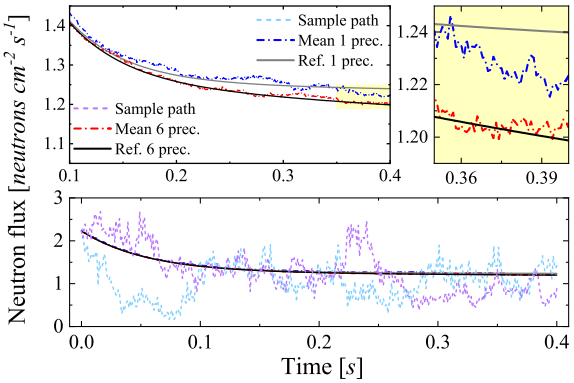

(b) Mean **fast** neutron fluxes and two sample paths for **negative** step reactivity.

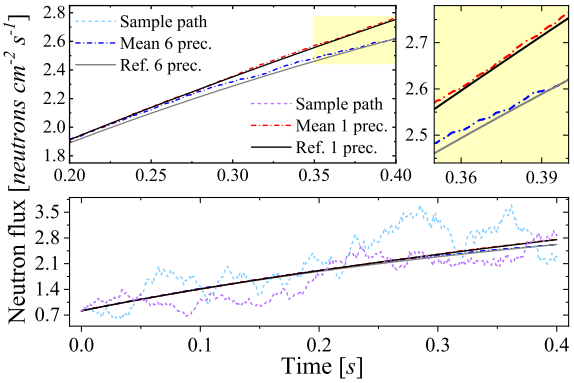

(c) Mean **thermal** neutron fluxes and two sample paths for **positive** step reactivity.

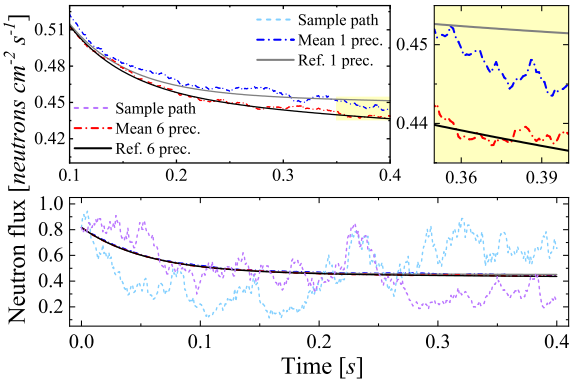

(d) Mean **thermal** neutron fluxes and two sample paths for **negative** step reactivity.

Figure 4.1: Neutron fluxes for **step** reactivity insertions with one and six groups of delayed neutrons. Light blue and light purple dashed lines stand for the sample path for 1 and 6 precursors, respectively. Also, blue and red dashed lines represent the mean values for 1 and 6 precursors, respectively; while the gray and black solid lines give the reference values for 1 and 6 precursors, respectively. Inset at right shows a zoom of the yellow shaded region at left.

Table 4.3: Data for the fast and thermal neutron fluxes using one and six precursors groups for negative step reactivity.

	Method		Time [s] 0.00	0.05	0.10	0.15	0.20	0.30	0.40
One Precursor	**AMF**	Fast	2.228929	1.645481	1.409437	1.313217	1.273214	1.247508	1.239679
		Thermal	0.816356	0.601048	0.513969	0.478479	0.463731	0.454268	0.451400
	This work	Fast	2.228929	1.664219	1.432717	1.323924	1.284070	1.254850	1.223374
			(NA)	*(0.740093)*	*(0.716911)*	*(0.683589)*	*(0.682731)*	*(0.647724)*	*(0.638791)*
		Thermal	0.816356	0.607165	0.522997	0.482617	0.468556	0.456693	0.445028
			(NA)	*(0.262793)*	*(0.255943)*	*(0.244702)*	*(0.242443)*	*(0.230407)*	*(0.226891)*
Six Precursors	**AT***	Fast	2.228929	1.644662	1.405236	1.303591	1.257209	1.218425	1.198645
		Thermal	0.816356	0.600760	0.512464	0.475006	0.457938	0.443711	0.436489
	This work	Fast	2.228929	1.652668	1.404029	1.312502	1.257231	1.219096	1.203751
			(NA)	*(0.568092)*	*(0.561540)*	*(0.540936)*	*(0.536882)*	*(0.517206)*	*(0.516555)*
		Thermal	0.816356	0.603314	0.511551	0.478060	0.457749	0.444288	0.438643
			(NA)	*(0.201299)*	*(0.200864)*	*(0.194116)*	*(0.191520)*	*(0.184962)*	*(0.184731)*

$^*\alpha = 1$

4.1.2 Ramp Reactivity

As a second case study we consider a time-dependent reactivity insertion[5], through a perturbation in the thermal group absorption cross-section given by $\Delta\Sigma_{2,a} = \pm 0.369 \times 10^{-4} T^{-1} t \ cm^{-1}$. **Tables 4.4** and **4.5** report on the results of fast and thermal neutron fluxes. Reference values for positive and negative ramp reactivities with six groups of delayed neutrons were taken from the work of Aboanber *et. al* [57], where the numerical solutions are obtained through the Magnus Expansion Method (MEM). For positive and negative ramp reactivities with one group of delayed neutrons we compare with references [35] and [58], which report results from a Generalization of the Analytical Exponential Model (GAEM) and the Fundamental Matrix Method (FMM), respectively. The model under study in the last three related works coincides with the deterministic one considered in this study (described in Chap. 2).
Again, IEM (this work) yields accurate results, with percentage errors below 1.3%. **Figure 4.2**, shows that, for negative insertion, the mean values present bigger fluctuations than for positive insertion case.

Table 4.4: Data for the fast and thermal neutron fluxes using one and six precursors groups for positive ramp reactivity.

	Method		Time [s] 0.00	0.05	0.10	0.15	0.20	0.30	0.40
One Precursor	**FMM**	Fast	2.228930	2.276754	2.399141	2.580130	2.816688	3.484223	4.529887
		Thermal	0.816356	0.834008	0.879171	0.945956	1.033243	1.279550	1.665373
	This work	Fast	2.228930	2.299019	2.432781	2.604321	2.850085	3.524813	4.510834
			(NA)	*(0.966116)*	*(1.157748)*	*(1.299797)*	*(1.464997)*	*(1.782104)*	*(2.303448)*
		Thermal	0.816356	0.841289	0.892268	0.955165	1.046904	1.294013	1.657626
			(NA)	*(0.345543)*	*(0.418621)*	*(0.471711)*	*(0.531014)*	*(0.648673)*	*(0.839914)*
Six Precursors	**MEM***	Fast	2.228930	2.276699	2.399435	2.581859	2.821866	3.507541	4.601092
		Thermal	0.816356	0.833988	0.879276	0.946579	1.035121	1.288051	1.691415
	This work	Fast	2.228930	2.283240	2.395160	2.594450	2.823642	3.511691	4.627514
			(NA)	*(0.740631)*	*(0.909801)*	*(1.027921)*	*(1.166121)*	*(1.456732)*	*(1.939770)*
		Thermal	0.816356	0.835944	0.877060	0.950923	1.035483	1.290072	1.701669
			(NA)	*(0.264466)*	*(0.328995)*	*(0.373987)*	*(0.423206)*	*(0.531257)*	*(0.710016)*

$^*3^{th}$ approximation

[5]These types of perturbation are typically generated by the movement of control rods in the reactor.

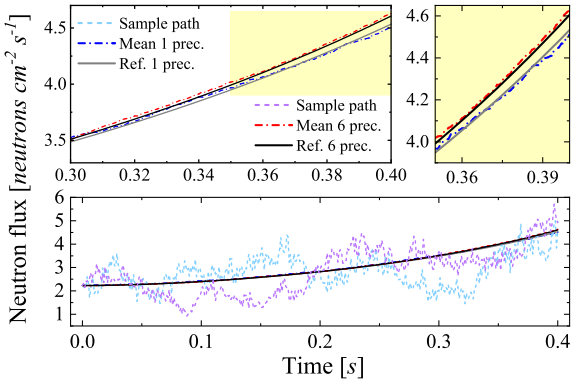

(a) Mean **fast** neutron fluxes and two sample paths for **positive** ramp reactivity.

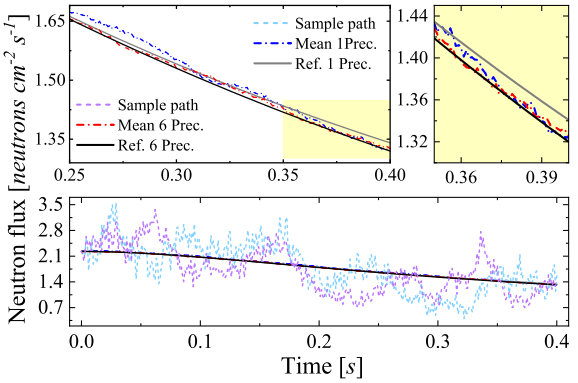

(b) Mean **fast** neutron fluxes and two sample paths for **negative** ramp reactivity.

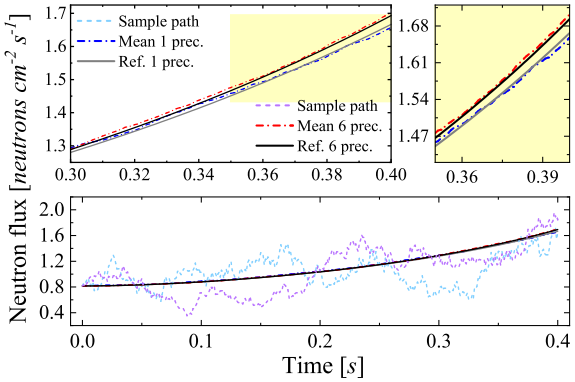

(c) Mean **thermal** neutron fluxes and two sample paths for **positive** ramp reactivity.

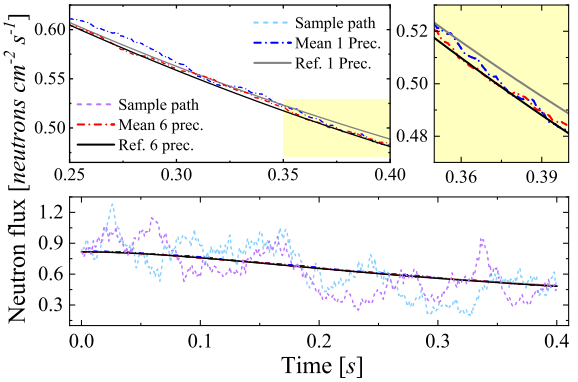

(d) Mean **thermal** neutron fluxes and two sample paths for **negative** ramp reactivity.

Figure 4.2: Neutron fluxes for **ramp** reactivity insertions with one and six groups of delayed neutrons. Light blue and light purple dashed lines stand for the sample path for 1 and 6 precursors, respectively. Also, blue and red dashed lines represent the mean values for 1 and 6 precursors, respectively; while the gray and black solid lines give the reference values for 1 and 6 precursors, respectively. Inset at right shows a zoom of the yellow shaded region at left.

Table 4.5: Data for the fast and thermal neutron fluxes using one and six precursors groups for negative ramp reactivity.

			Time [s]						
	Method		0.00	0.05	0.10	0.15	0.20	0.30	0.40
One Precursor	**GAEM**	Fast	2.228929	2.182170	2.072892	1.936528	1.795460	1.541033	1.340396
		Thermal	0.816356	0.799097	0.758773	0.708456	0.656407	0.562539	0.488524
	This work	Fast	2.228929	2.202359	2.101324	1.952671	1.813443	1.552836	1.324255
			(NA)	*(0.930556)*	*(1.010642)*	*(0.986931)*	*(0.948472)*	*(0.795450)*	*(0.688733)*
		Thermal	0.816356	0.805631	0.769875	0.714649	0.664067	0.566571	0.482192
			(NA)	*(0.332483)*	*(0.364297)*	*(0.356394)*	*(0.340473)*	*(0.284795)*	*(0.245198)*
Six Precursors	**MEM***	Fast	2.228930	2.182266	2.072701	1.935227	1.791970	1.530218	1.320096
		Thermal	0.816356	0.799131	0.758705	0.707989	0.655146	0.558618	0.481157
	This work	Fast	2.228930	2.187289	2.067262	1.944171	1.791222	1.530826	1.325908
			(NA)	*(0.713496)*	*(0.793953)*	*(0.780900)*	*(0.752101)*	*(0.642766)*	*(0.563829)*
		Thermal	0.816356	0.800539	0.756113	0.711024	0.654638	0.559200	0.483586
			(NA)	*(0.254500)*	*(0.286322)*	*(0.282726)*	*(0.270692)*	*(0.231166)*	*(0.202135)*

$^*3^{th}$ approximation

4.1.3 Sinusoidal Reactivity

As a last case study we consider a positive sinusoidal insertion[6]. This time we take into account a perturbation in the thermal group absorption cross-section given by

[6]This type of perturbation can occur due to control rod oscillations or certain mechanisms involving temperature, such as the appearance of bubbles that avoids proper heat transfer. Perturbations of this type have

$\Delta\Sigma_{2,a} = -0.369 \times 10^{-4} sin\,(2\pi\tau^{-1}t)\ cm^{-1}$, with $\tau = 0.8$ and $\tau = 0.4$ seconds for one and six groups of delayed neutrons.

Table 4.6 reports on the results of fast and thermal neutron fluxes. Reference values for one group of delayed neutrons were compared to the MEM method; while, for six groups of delayed neutrons the results were compared with the AT method. On this respect, **Fig. 4.3** shows the mean values for the neutron flux using one and six groups of delayed neutrons. It is observed that bigger random fluctuations are obtained when the population changes its trend, as occurs in the peak and valley sectors. This behavior is due to the sudden change in reactivity, which explains why the constant insertion presents both a greater error percentage and fluctuations in the mean values than the time-dependent case.

Table 4.6: Data for the fast and thermal neutron fluxes using one and six precursors groups for sinusoidal reactivity.

			Time [s]						
	Method		0.00	0.05	0.10	0.15	0.20	0.30	0.40
One Precursor $\tau = 0.8\ sec$	**MEM***	Fast	2.228930	2.380577	2.780147	3.372849	4.070518	4.969714	3.996805
		Thermal	0.816356	0.872330	1.019779	1.238484	1.495907	1.827613	1.468507
	This work	Fast	2.228930	2.405608	2.821164	3.409460	4.125541	5.030763	3.979153
			(NA)	*(1.005121)*	*(1.328297)*	*(1.680312)*	*(2.090015)*	*(2.534381)*	*(2.037490)*
		Thermal	0.816356	0.880611	1.035679	1.252328	1.517893	1.849521	1.461325
			(NA)	*(0.359871)*	*(0.481604)*	*(0.611966)*	*(0.761754)*	*(0.926165)*	*(0.741932)*
Six Precursors $\tau = 0.4\ sec$	**AT**†	Fast	2.228930	2.530834	3.247809	3.855372	3.645454	1.925300	1.700186
		Thermal	0.816356	0.927785	1.192325	1.416411	1.338814	0.704067	0.621142
	This work	Fast	2.228930	2.541330	3.246943	3.870004	3.639474	1.926468	1.711538
			(NA)	*(0.812859)*	*(1.202982)*	*(1.494957)*	*(1.472138)*	*(0.796306)*	*(0.713571)*
		Thermal	0.816356	0.931181	1.191251	1.421452	1.336272	0.704889	0.625654
			(NA)	*(0.291000)*	*(0.436984)*	*(0.546504)*	*(0.535798)*	*(0.287595)*	*(0.257383)*

*2^{nd} approximation. †$\alpha = 1$

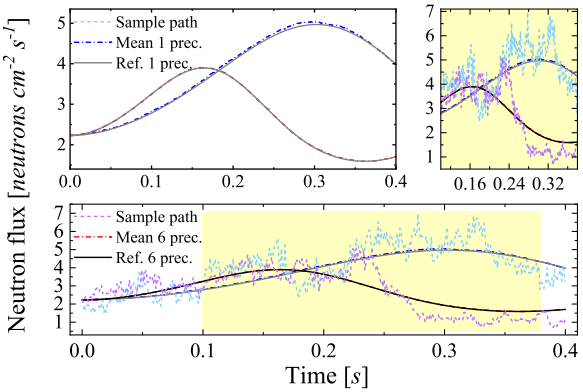

(a) Mean **fast** neutron fluxes and two sample paths for sinusoidal reactivity.

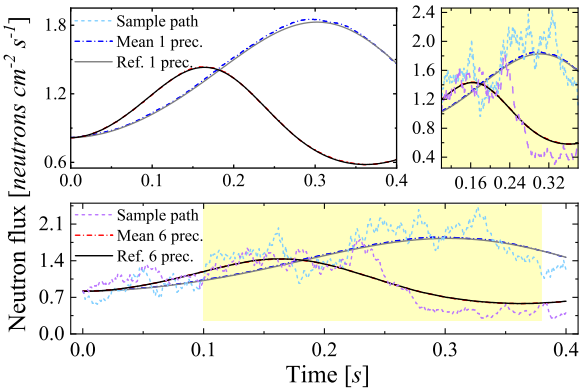

(b) Mean **thermal** neutron fluxes and two sample paths for sinusoidal reactivity.

Figure 4.3: Neutron fluxes for positive **sinusoidal** reactivity insertions with one and six groups of delayed neutrons. Light blue and light purple dashed lines stand for the sample path for 1 and 6 precursors, respectively. Also, blue and red dashed lines represent the mean values for 1 and 6 precursors, respectively; while the gray and black solid lines give the reference values for 1 and 6 precursors, respectively. Inset at right shows a zoom of the yellow shaded region at bottom.

been observed recently in the German KWU reactors [59, 26, 27]

As observed from subsections 4.1.1 to 4.1.3, in this first reactor, the calculations of the neutron populations through the proposed stochastic model are in very good agreement with the reference values, regardless the different numerical schemes and various modeling methodologies employed. Indeed, the errors found are small; although they could slightly vary depending on the pseudo-random numbers used to generate the Wiener processes.

From other side, the sample paths reported in **Figs. 4.1**, **4.2**, and **4.3** reveal a clue result. In recent works, stability of the stochastic Point Kinetics equations models has been discussed. In particular, discussions about the realizations of the stochastic process [60, 61] have been presented, correctly arguing that they do not represent the reactor behavior since, due to the random behavior, they would imply random reactor meltdowns and shutdowns, something that is not observed; see, for example, references [24, 61] and elsewhere. Here, we can solve this drawback since all the random variables described in Chap. 2 are identically distributed, hence the Central Limit Theorem takes on the form seen in Eqn. (2.34), which differs from other models by the $n^{-1/2}$ factor that accompanies the covariance matrix, whose presence reduces the extreme random fluctuations of the stochastic realizations. Conversely to previous models, with ours, no meltdowns or shutdowns are obtained in the reactor description. Although in the related figures the random fluctuations appear as large at some extent, they can be attenuated when effects such as thermal feedback, or heat transport mechanisms are considered within the model, as shown by Stein and Dubi [60].

In the next section, an actual nuclear reactor scenario is considered, and the stochastic model is tested against experimental results.

4.2 REAL NUCLEAR REACTOR (AGN-201)

The second thermal nuclear reactor we consider in this study for comparison purposes is the AGN-201. It is a real nuclear reactor consisting of a cylinder 25.6 cm in diameter and 24.0 cm height, whose core material is a homogeneous mixture of polyethylene and uranium dioxide [62]. **Table 4.7** shows the reactor parameters, which have been taken from the Cooke's work and the Zohuri's book [63, 11].

Table 4.7: Parameters of a cylindrical AGN-201 reactor.

Parameter	Fast neutrons	Thermal neutrons	Delayed group i	λ_i $[s^{-1}]$	β_i $(\times 10^{-2})$
D $[cm^{-1}]$	0.623000	0.125000	1	0.0124	0.0210
$\Sigma_a[cm^{-1}]$	0.001542	0.076558	2	0.0205	0.1400
$\nu\Sigma_f[cm^{-1}]$	0.002562	0.151790	3	0.1110	0.1250
$\Sigma_s[cm^{-1}]$	0.055110	-	4	0.3010	0.2530
v $[cm\,s^{-1}]$	3.00×10^{7}	2.68×10^{5}	5	1.1400	0.0740
k_{eff}	1.00		6	3.0100	0.0270
T_c [°C]	3.00		*average*	*0.07675*	
α_T [°C^{-1}]	-2.75×10^{-4}		γ [s^{-1}]	1.00×10^{-4}	
K $[cm^3\,°C\,neut^{-1}\,s^{-1}]$	2.31×10^{-7}				

4.2.1 Drop Test

In 1961, Cooke reported results from the rod drop test experiment, which consists of approximating negative step reactivity by inserting a control element into the reactor as fast as possible [64, 65]. In this case, a polyethylene rod is quickly inserted into the reactor through a 2.54 cm in diameter hole known as the *glory hole*[7], while the reactor is at steady power. This experiment allows to know the maximum quantity of available reactivity of the control elements through the following expression:

$$\rho\beta_{\text{eff}}^{-1} = \frac{N_1(t) + N_2(t)}{N_1(t+\Delta t) + N_2(t+\Delta t)}\beta k_{\text{eff}}^{-1}, \tag{4.1}$$

where, $\rho\beta_{\text{eff}}^{-1}$ is the quantity of reactivity known as *One Dollar* (represented by \$), which can also be expressed in "per cent mille" represented by *pcm* (with $pcm = 10^5$ \$); $N_g(t)$ and $N_g(t+\Delta t)$ are the neutron densities at steady power and once the control element is fully inserted, respectively. From this experiment, the effective delayed neutron fraction (β_{eff}) can also be determined. This is a key parameter in reactor safety, which measures the capacity of the reactor to thermalize neutrons [66].

Here, we simulated the steady state of the reactor during 0.5 seconds. After this, a step negative reactivity of 2% of the initial thermal reactivity was introduced. In addition, once the perturbation was introduced, an external source of neutrons $\vec{Q}_t = [q_1\ q_2]^T$, with $q_1 = 375\ neutrons\ cm^{-3}s^{-1}$ and $q_2 = 0.2\ q_1$, was considered. This simulates neutrons coming from the reactor's reflective barriers. After the perturbation, the reactor is allowed to evolve for 7.5 s longer. For calculations, a time step of 3 ms and 250 stochastic realizations were used with six groups of delayed neutrons, and initial conditions given by: $N_1(0) = 5.1652$, $N_2(0) = 2.8348$, and $c_i(0) = [\mu_{i,1}N_1(0) + \mu_{i,2}N_2(0)]\,\lambda_i^{-1}$.

The mean value of the maximum quantity of available reactivity of the polyethylene rod was $\rho\beta_{\text{eff}}^{-1} = 226$ *pcm* with 22 *pcm* as standard deviation. These values are in excellent agreement with the experimental Cooke's findings, namely 230 ± 20 *pcm*, as well as with the reference value of the course rod experiment also performed by Cooke with a different methodology which goes to 221 *pcm*, allowing to compute this same quantity. In this simulation, the effect of thermal feedback was considered, with 20 °C as initial temperature, the same temperature for the coolant, and a thermal reactivity temperature coefficient of $2500\,\alpha_T$. However, due to the small change observed in the neutron population, this effect can be neglected with no modifications in the calculations. Appendix A shows the MATLAB code used for this simulation.

Figure 4.4 shows comparisons between our results (solid dark blue line) for the rod drop test and the experimental curve (solid red line), which was obtained by a digitalization process from the original reference. The inset reports the values of $\rho\beta_{\text{eff}}^{-1}$ obtained by Cooke (light green) and this work (cyan dot). It is worth noticing that, in the experiment, a finite time is needed to introduce the polyethylene rod into the reactor, which causes the differences observed between our framework and the experimental curve. Thus, once the polyethylene rod is fully introduced, an extrapolation of the experimental curve, through the dashed red line, is done to compute the $\rho\beta_{\text{eff}}^{-1}$ value. Finally, the blue dots are the result of one of the

[7]See Fig. 3 in ref. [62] for a view of the AGN-201 core tank and its contents.

realizations of the stochastic process (sample path), whose fluctuations completely agree with those observed in the real measurements [64].

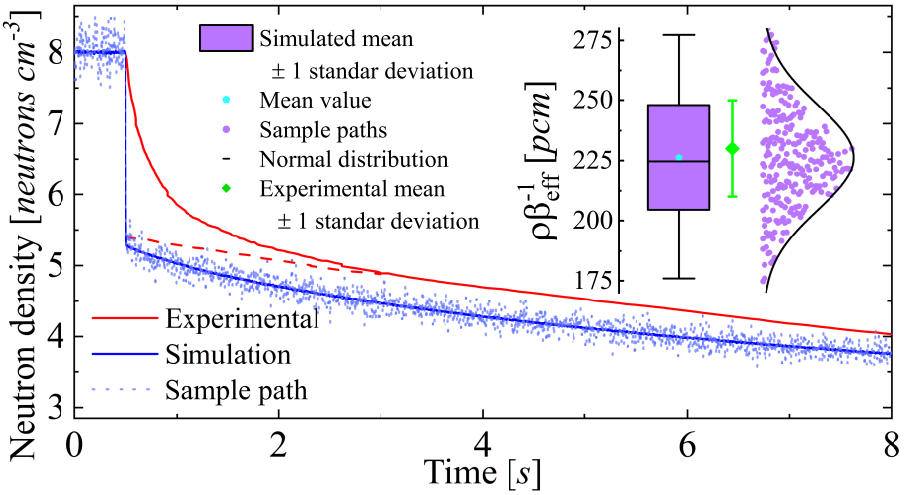

Figure 4.4: Total neutron density for the drop test. Inset shows the experimental value of $\rho\beta_{\text{eff}}^{-1}$ with their standard deviation (light green) [63], as well as our result (cyan dot with purple bar), and the distribution of the stochastic realizations for the $\rho\beta_{\text{eff}}^{-1}$ quantity.

4.2.2 Temperature Feedback

Conversely to the previous case, in this section, we show a scenario where the thermal feedback effect is non-negligible. For this purpose, we considered a ramp positive reactivity of 4% of the reactor thermal reactivity, of the form $\rho_{0,2}(t) = -0.04\rho_{2,0}\tau^{-1}t$, with $\tau = 92\,s$. The initial conditions were $N_1(0) = 9.68475$, $N_2(0) = 5.31525$, and $c_i(0) = [\mu_{i,1}N_1(0) + \mu_{i,2}N_2(0)]\,\lambda_i^{-1}$, with 0.034 $^\circ C$ and 3 $^\circ C$ as initial temperature of the reactor and coolant temperature, respectively. This simulation was performed in a time window of 170 seconds with a time step of 25 milliseconds and 50 realizations of the stochastic process.

Figure 4.5 shows the results of our simulation, where the dashed lines are the reference curves for total neutron density and the reactor temperature ($\times 100$) taken from the simulations carried out by Cooke through digitalization, while the solid lines represent results of this study. As observed, our result are in qualitative good agreement with the trends reported by Cooke (indeed, there are coincidences in the time interval which the neutron populations grows in, the maximum value of the population, and the decreasing population process due to thermal feedback), and the lack of complete coincidence among the curves can be ascribed to our ignorance of the exact parameters used by Cooke. A growth of the neutron population is observed during the initial 55 s due to the induced perturbation. At this time, reactor temperature increases considerably, thus activating the thermal feedback effect that prevents exponential growth and decreases the population for a few seconds. Then, after the peak of the neutron population at 55 seconds (with a value of 3.2476×10^6 $neutrons\,cm^{-3}$), a slightly increasing behavior is obtained. We also found close agreement between our total neutron density curve and that presented by Bogado *et. al* [52] and references therein. The inset shows the very initial time of the simulation, where the neutron population is low, and random fluctuations are noticeable. Again, as in the drop test case, the sample path fluctuates narrowly around the mean value, in close agreement with real experiments, differently from the other studied mod-

els which yield enormous fluctuations, well far from the real observations. This fact indicates the stability in the realizations of our stochastic model and its good quality for describing the real processes. These great advantages make our proposed methodology very appropriate for the study of these kind of systems.

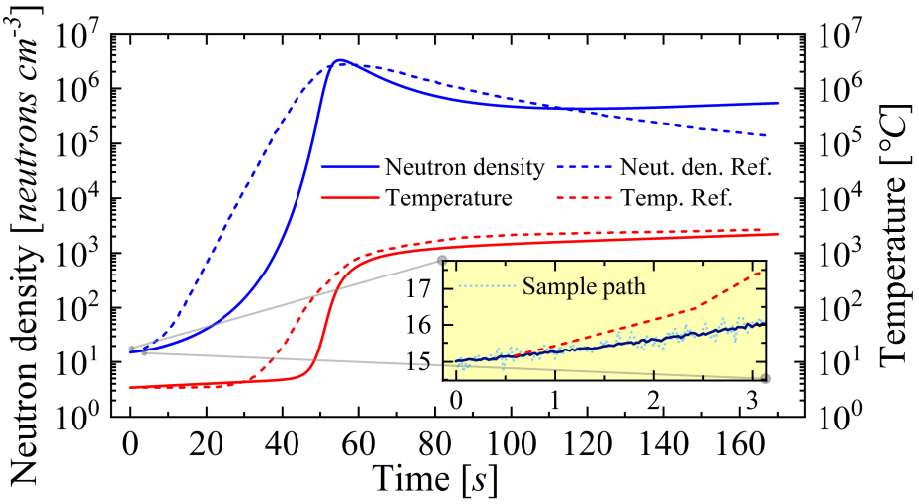

Figure 4.5: Total neutron density (blue solid curve and left-side axis) and temperature curve (red solid curve and right-side axis in units of $\times 100\,^{\circ}C$) for the case of positive ramp reactivity with temperature feedback effect. The dashed lines show the reference values taken for each case from the related Cooke's work [63]. Inset shows a zoom in of the curve at very small time.

Summing up, we have studied a real nuclear reactor through stochastic differential equations, which the energy variables was included in. Conversely, in the stochastic models reported so far only mono-energetic neutrons have been considered, which is far from reality, as discussed in Chap. 2. It is worth noting that the random variables describing the events that change the neutron population are independent and identically distributed, what allows the use of the Central Limit Theorem in the Lindeberg-Lévy form, and results in the appearance of the factor $n_e^{-1/2}$ in the co-variance matrix. Since $n_e^{-1/2} < 1$, the random fluctuations (noise) in the stochastic process are reduced. The fact that the random variables are identically distributed causes that our model does not present the *instability* shown in previous models [60, 61]. Indeed, these authors report that the stochastic models exhibit excessive noise, and their realizations predict random shutdowns and meltdowns events, which does not occur in real operation of the reactors.

Aiming to illustrate this situation, **Fig.4.6(a)** shows the AGN-201 reactor at steady-state as well as the comparison of two realizations of the stochastic process (sample paths). One of those realizations comes from our model (identically distributed variables and Lindeberg-Lévy form of the CLT), while the other one is coming from previous models where the Lyapunov form of the CLT is used. As observed, fluctuations in the results of our model are four times smaller than those in the other one for the same Wiener process. This meaningful decrease in noise allows using a smaller number of realizations of the stochastic process to obtain accurate results. This fact is clearly illustrated in **Fig. 4.6(b)**, which shows the maximum excess reactivity of the polyethylene rod in the AGN-201 reactor computed by our model, correctly

matching experimental data (represented by the orange shaded area). Contrarily, previous models present excessive standard deviations.

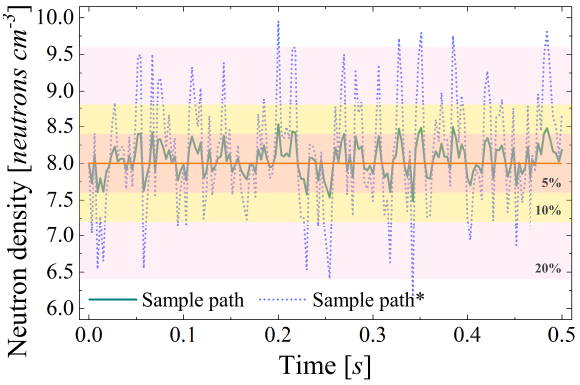

(a) AGN-201 nuclear reactor at steady state and two sample paths of the stochastic process using Lindeberg-Lévy (green solid line) and Lyapunov* central limit theorem (blue doted line) are shown.

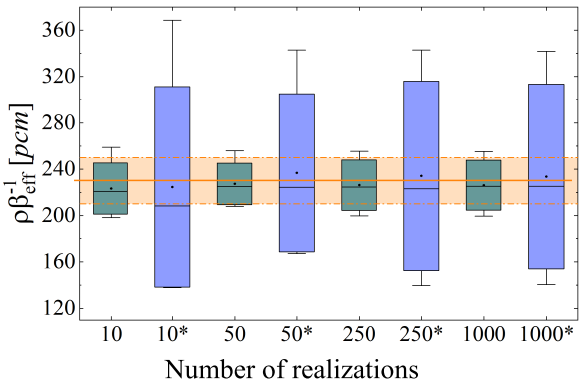

(b) Maximum excess reactivity available in the polyethylene rod as a function of the number of realizations of the stochastic process using Lindeberg-Lévy (dark green bars) and Lyapunov* central limit theorem (blue bars).

Figure 4.6: AGN-201 nuclear reactor simulations for: (a) A steady state scenario at a neutron density of 8 *neutrons* cm^{-3} (orange solid line), two sample paths of the stochastic process using Lindeberg-Lévy (green solid line) and Lyapunov (blue doted line) forms of the central limit theorem. Color shaded areas represent different error percentages. (b) Maximum excess reactivity $\rho\beta^{-1}_{\text{eff}}$ using Lindeberg-Lévy (green bars) and Lyapunov (blue bars) central limit theorem. Black dots stand for mean values, bars represent one standard deviation, and black whiskers range from 10 to 90 of the simulated data. The orange shaded area represent experimental values, with the solid line showing the mean value, and the dashed lines indicating 1 standard deviation.

5. CONCLUSIONS

In this research, the stochastic model of the Point Kinetics equations with two-energy groups and multi-groups of delayed neutrons has been derived in detail, taking into account the thermal feedback effect. The Euler-Maruyama scheme in implicit form was proposed to approximate numerical solutions since the model studied lacks analytical solutions.

Our model results were compared with two thermal nuclear reactors. The first one represents a hypothetical reactor in which different types of perturbations were considered. Mean values of the stochastic model were found in excellent agreement with those reported in the literature, which employ diverse numerical techniques and several methodologies for nuclear reactor modeling.

The second case selected was a real reactor of type AGN-201. In this case, the rod drop test was simulated. Mean value and standard deviation results show an overall good agreement with experimental data. A valuable advantage of our model is that, conversely to other deterministic and widely used models, it provides approximations to the standard deviations, thus showing that stochastic models are more general than deterministic ones. Furthermore, our model solves the instability of the stochastic realizations presented by previous frameworks.

These comparisons allow us to conclude that the proposed stochastic model can be considered as an appropriate and very useful tool to describe the behavior of nuclear reactors by using the appropriate initial conditions and reactor configurations.

As perspectives for future works, it is open the possibility of presenting a generalization of this model by including space as a variable in the reactor description, so as to distinguish its different zones, such as reflective barriers, irradiation channels, control zones, among others.

In addition, more physical rigor could also be included in the model, by, for example, adding more energy-groups, considering thermo-hydraulic effects involved in cooling, studying poisoning effects. Given the limited availability of experimental data in the literature, the Colombian TRIGA nuclear reactor would be a good option for obtaining data for comparison purposes given its well-known design. Clearly, this could imply a great deal of research and technological development for our country.

APPENDIX A. PUBLICATIONS

As result of the research work developed during this Master program, we have submitted for publication to the journal *Progress in Nuclear Energy*, the manuscript entitled:

1. *THETA METHOD APPLIED TO TWO-ENERGY GROUPS POINT KINETICS EQUATIONS*, by Daniel E. Cedeño-Girón, Abdallah A. Nahla and J. Mazo-Zuluaga.

Currently, we are also writing the final part of the manuscript entitled:

2. *STOCHASTIC POINT REACTOR KINETICS EQUATIONS WITH TWO-ENERGY GROUPS*, by Daniel E. Cedeño-Girón, Rodrigo Henao-Henao and J. Mazo-Zuluaga, which will also be promptly submitted to *Progress in Nuclear Energy*.

APPENDIX B. MATLAB CODE

MATLAB code for the rod drop test.

```
clear, clc
tstart = cputime;

%% Study Interval
T = 8 ;                    %Length of Time Interval
iterations = 330*T ;       %Number of Iterations
h = T/iterations ;         %Time Step
t = 0:h:T ;                %Time

%% Experiment Parameters
g = 2 ;                    %# of Energy groups
m = 6 ;                    %# of Precursors
n = m + 3*g + (g-1) ;      %# random variables
high=24 ; diameter=25.6 ; Vol=pi*high*(diameter/2)^2 ;  %Volume of reactor core
if (m==1), L = 0.07675; B = 0.0064; BettaT = B ;
elseif (m==6), L = [ 0.0124 0.0205 0.1110 0.3010 1.1400 3.0100 ] ;  %i-th Decays Constants
               B = [ 0.21 1.40 1.25 2.53 0.74 0.27 ]*10^-3 ;  %i-th fraction of precursor
                   group
               BettaT = 0;
               for i=1:m, BettaT = BettaT + B(1,i); end, end  %Total Fraction of precursor
                   group
nu = 2.41 ;                %Average # of Neutron Generate per Fission Event
D = [0.623 0.125] ;        %Diffusion Coefficients
v = [30 0.268]*10^6 ;      %Speed of Neutrons
Keff = 1.0 ;
SgF = [0.002562 0.151790]/(nu*Keff) ;  %nuFission Cross-Section
SgS = 0.05511 ;                        %Scattering Cross-Section
SgA = [0.002004 0.099500] ;            %Absortion Cross-Section
q = - [375 75] ;                       %Intensity Neutron Source

%% New Experiment Parameter
LM = [1/(nu*SgF(1)*v(1)) 1/(nu*SgF(2)*v(2))];  %Generation Time of Neutrons
mu = zeros(6,2) ; for i=1:m, for j=1:2, mu(i,j) = B(i)/LM(j) ; end, end

%% Initial Conditions
N = [5.1652 2.8348]*Vol ;  %# of Fast and Thermal Neutrons
C=zeros(1,m); for i=1:m, C(i) = ( mu(i,1)*N(1) + mu(i,2)*N(2) )/L(i) ; end  %# of i-th
    Precursor
X=zeros(m+2,iterations+1);
if (m==1), X(:,1) = [N(1); N(2); C(1)] ;
elseif (m==6), X(:,1) = [N(1); N(2); C(1); C(2); C(3); C(4); C(5); C(6)] ; end  %Vector of
    random Variables

%% Buckling of material Squared
Bm1 = - (SgA(1)+SgS)/D(1) + ( nu*SgF(1)*v(1)*N(1) + nu*SgF(2)*v(2)*N(2) )/( D(1)*v(1)*N(1) )
    ;  %Fast
Bm2 = - SgA(2)/D(2) + ( SgS*v(1)*N(1) )/( D(2)*v(2)*N(2) ) ;  %Thermal

%% Reactivity
rho1 = 1 - (SgA(1) + D(1)*Bm1)/(nu*SgF(1)) ;  %Fast
rho2 = zeros(1,iterations+1) ; rho2(1,1) = 1 - (SgA(2) + D(2)*Bm2)/(nu*SgF(2)) ;  %Thermal

%% Feedback Temperature Effects on Reactivity
Temp=zeros(1,iterations+1) ;  Temp(1,1) = 20 ;    %Inital Temperature
Tc = 20 ;                                         %Coolant Temperature
```

```
alphaT = - 2.75*1E-4 ;                          %Temperature coefficient of reactivity
K = 2.31*1E-7 ;                                 %Reciprocal of the thermal capacity of the
    reactor
gammaT = 1E-4 ;                                 %Mean time for heat transfer to coolant^-1

%% Elements of Matrix A
k = v(1)*SgS ;
alpha = ( BettaT - rho1 )/LM(1) + k ;
zeta = ( 1 - BettaT )/LM(2) ;

%% Wiener's Processes
MB = 250 ;              %# of Wiener Processes
seed = 2794 ;           %Seed (generate the same random numbers)
rng(seed,'twister');  %random number generator
WIN = zeros(MB,iterations+1); E=zeros(1,m); EE=zeros(1,m); M = zeros(m+2,m+2);
for j=1:MB
    %% Differential Wiener Processes with mean 0 and var 1
    DW = sqrt(h)*randn(n,iterations+1) ;
for i=1:iterations
    %% Perturbation
    if (i<166), Q = zeros(m+2,1) ;
        rho2(1,i) = 1 - (SgA(2) + D(2)*Bm2)/(nu*SgF(2)) ;
    elseif (i==166) && (m==1)
        rho2(1,i+1) = 1.002*rho2 ;
        Q = [ q(1); q(2); 0 ]*Vol ;  %Neutron Source
    elseif (i==166) && (m==6)
        rho2(1,i+1) = 1.002*rho2 ;
        Q = [ q(1); q(2); 0; 0; 0; 0; 0; 0 ]*Vol ;  %Neutron Source
    end

    eta = (1 - rho2(1,i+1))/LM(2) ;
    %% Analytical Matrix M=(I-A*h)^-1
    theta = 1/( 1 + h*eta ) ;
    for r=1:m, EE(r) = h*mu(r,2)*theta/( 1 + h*L(r) ) ; end
    for r=1:m, E(r) = ( h*mu(r,1) + h*h*mu(r,2)*k*theta )/( 1 + h*L(r) ) ; end
    suma1=0; for r=1:m, suma1 = suma1 + L(r)*E(r) ; end
    suma2=0; for r=1:m, suma2 = suma2 + L(r)*EE(r) ; end
    M(1,1) = 1/( 1 + h*alpha - h*h*zeta*k*theta - h*suma1 ) ;
    M(1,2) = ( h*zeta*theta + h*suma2 )*M(1,1) ;
    for r=1:2, M(2,r) = h*k*theta*M(1,r) ; if (r==2), M(2,r) = M(2,2) + theta ; end, end
    for r=1:m
        M(1,r+2) = h*L(r)*M(1,1)/( 1 + h*L(r) ) ;
        M(2,r+2) = h*k*theta*M(1,r+2) ;
        M(r+2,1) = E(r)*M(1,1) ;
        M(r+2,2) = EE(r) + E(r)*M(1,2) ;
        for s=1:m, M(r+2,s+2) = E(r)*M(1,s+2) ; M(s+2,r+2) = E(s)*M(1,r+2) ;
            if (r==s), M(r+2,s+2) = E(r)*M(1,s+2) + 1/( 1 + h*L(r) ) ; end, end
    end

    %% Diffusion Tensor
    G=zeros(m+2,n);
    Sf = SgS/(nu*SgF(1)) ;
    %% Death Due to Radioactive Capture
    G(1,1) = - real( sqrt( X(1,i)*( 1 -rho1 - 1/nu )/LM(1) ) ) ;  %Death Fast Group
    G(2,2) = - real( sqrt( X(2,i)*( 1 -rho2(1,i) - 1/nu )/LM(2) ) ) ;  %Death Thermal Group
    %% Born due to Source
    G(1,3) = q(1) ; %Born in Fast Group
    G(2,4) = q(2) ; %Born in Thermal Group
    %% Born Due to Decays
    for r=1:m, G(1,r+4) = sqrt( L(r)*X(r+2,i) ) ; end  %Born in Fast Group
    for r=1:m, G(r+2,r+4) = - G(1,r+4) ; end           %Death of i-th Precursor

    if (m==1)
        %% Born in Thermal Group Due to Scattering
        G(1,6) = - sqrt( X(1,i)*Sf/LM(1) ) ;  %Death in Fast Group
        G(2,6) = - G(1,6) ;                   %Born in Thermal Group
        %% Fissions
        G(1,7) = ( - 1 + (1-BettaT)*nu )*sqrt( X(1,i)/( nu*LM(1) ) ) ;
        for r=1:m, G(r+2,7) = B(r)*nu*sqrt( X(1,i)/( nu*LM(1) ) ) ; end
        G(1,8) = (1-BettaT)*nu*sqrt( X(2,i)/( nu*LM(2) ) ) ;
        G(2,8) = - sqrt( X(2,i)/( nu*LM(2) ) ) ;
        for r=1:m, G(r+2,8) = B(r)*nu*sqrt( X(2,i)/( nu*LM(2) ) ) ; end
```

```
122
123     elseif (m==6)
124         %% Born in Thermal Group Due to Scattering
125         G(1,11) = - sqrt( X(1,i)*Sf/LM(1) ) ;  %Death in Fast Group
126         G(2,11) = - G(1,11) ;                  %Born in Thermal Group
127         %% Fissions
128         G(1,12) = ( - 1 + (1-BettaT)*nu )*sqrt( X(1,i)/( nu*LM(1) ) ) ;
129          for r=1:m, G(r+2,12) = B(r)*nu*sqrt( X(1,i)/( nu*LM(1) ) ) ; end
130         G(1,13) = (1-BettaT)*nu*sqrt( X(2,i)/( nu*LM(2) ) ) ;
131         G(2,13) = - sqrt( X(2,i)/( nu*LM(2) ) ) ;
132          for r=1:m, G(r+2,13) = B(r)*nu*sqrt( X(2,i)/( nu*LM(2) ) ) ; end, end
133
134     %% Implicit Euler-Maruyama Method
135     X(:,166) = X(:,1) ;
136     X(:,i+1) = M*( X(:,i) + h*Q*exp( (0.5-t(i+1))/10 ) + G*DW(:,i)/sqrt(n) ) ;
137
138     %% Feedback Temperature
139     rho2(1,i+1) = rho2(1,i) ...
140                   + h*2.5E3*alphaT*K*exp( - gammaT*( t(i)+t(i+1) )/2 )*( X(2,i)+X(2,i+1) )
                          /(2*Vol) ;
141     %% Temperature
142     Temp(1,i+1) = Temp(1,i) + h*( K*( X(2,i)/Vol + X(1,i)/Vol ) - gammaT*( Temp(1,i) - Tc ) )
            ;
143
144 end
145     %% Process Realization
146     WIN(j,:)=(X(1,:)+X(2,:))/Vol;  %Total Neutron Density
147 end
148
149 %% Reactivity/Delayed Neutron Effectiveness
150 WC = zeros(MB,1); for i=1:MB, WC(i,1)=( 8/WIN(i,202)  - 1 )*BettaT/Keff; end
151 Count = mean(WC) ;  StdCount = std(WC) ;  %Mean and Standard Deviation
152
153 %% Neutron Density
154 EN= mean(WIN) ;  StdN= std(WIN) ;  %Mean and Standard Deviation
155
156 %% Table
157 Table = [ Count StdCount ; EN(1,202) StdN(1,202) ] ;
158
159 tend = cputime - tstart;
```

REFERENCES

[1] I. Arto, I. Capellán-Pérez, R. Lago, G. Bueno, and R. Bermejo. The energy requirements of a developed world. *Energy for Sustainable Development*, 33:1–13, 2016. doi:http://dx.doi.org/10.1016/j.esd.2016.04.001.

[2] R. U. Ayres and J. C. J. M. Van den Bergh. The underestimated contribution of energy to economic growth. *Structural Change and Economic Dynamics*, 27:79–88, 2013. doi:http://dx.doi.org/doi:10.1016/j.strueco.2013.07.004.

[3] S. C. Bhattacharyya. Energy access programmes and sustainable development: A critical review and analysis. *Energy for Sustainable Development*, 16(3):260–271, 2012. doi:https://doi.org/10.1016/j.esd.2012.05.002.

[4] S. C. Bhattacharyya and S. Ohiare. The chinese electricity access model for rural electrification: Approach, experience and lessons for others. *Energy Policy*, 49:676–687, 2012. doi:https://doi.org/10.1016/j.enpol.2012.07.003.

[5] V. Knapp and D. Pevec. Promises and limitations of nuclear fission energy in combating climate change. *Energy Policy*, 120:94–99, 2018. doi:https://doi.org/10.1016/j.enpol.2018.05.027.

[6] J. Parsons, J. Buongiorno, M. Corradini, and D. Petti. A fresh look at nuclear energy. *Science*, 363(6423):105, 2019. doi:https://doi.org/10.1126/science.aaw5304.

[7] J. J. Duderstadt and L. J. Hamilton. *Nuclear Reactor Analysis*. John Wiley & Sons, Inc., New York, 1976.

[8] J. R. Lamarsh and A. J. Baratta. *Introduction to Nuclear Engineering*. Prentice-Hall, Inc, New Jersey, 3rd edition, 2001.

[9] S.R. Shimjith, A.P. Tiwari, and B. Bandyopadhyay. *Modeling and Control of a Large Nuclear Reactor: A three-Time-Scale Approach*. Springer, Berlin, 2013.

[10] M. Zarei. A multi-point kinetics based MIMO-PI control of power in PWR reactors. *Nuclear Engineering and Design*, 328:283–291, 2018. doi:https://doi.org/10.1016/j.nucengdes.2018.01.011.

[11] B. Zohuri. *Neutronic Analysis for Nuclear Reactor Systems*. Springer, Cham, 2nd. edition, 2019.

[12] C. M. Cooling, M. M. R. Williams, E. T. Nygaard, and M. D. Eaton. The application of polynomial chaos methods to a point kinetics model of MIPR: An aqueous homogeneous reactor. *Nuclear Engineering and Design*, 262:126–152, 2013. doi:https://doi.org/10.1016/j.nucengdes.2013.03.055.

[13] T. J. Dolan. *Molten Salt Reactors and Thorium Energy*. Elsevier Ltd, United Kingdom, 2017.

[14] D. M. Pérez, D. E. M. Lorenzo, C. A. de Oliveira Lira, and L. P. G. Rodríguez. Neutronic evaluation of the steady-state operation of a 20kWth aqueous homogeneous reactor for Mo-99 production. *Annals of Nuclear Energy*, 128:148–159, 2019. doi:https://doi.org/10.1016/j.anucene.2019.01.002.

[15] H. Khodadadi and N. Ayoobian. Conceptual design and uncertainty analysis of a typical 50kW aqueous homogeneous reactor aimed for medical isotope production. *Progress in Nuclear Energy*, 121:103233, 2020. doi:https://doi.org/10.1016/j.pnucene.2019.103233.

[16] A.F. Henry. The application of reactor kinetics to the analysis of experiments. *Nuclear Science and Engineering*, 3(1):52–70, 1958. doi:http://dx.doi.org/10.13182/NSE58-1.

[17] A. Pungerčič, D. Čalič, and L. Snoj. Computational burnup analysis of the TRIGA Mark II research reactor fuel. *Progress in Nuclear Energy*, 130:103536, 2020. doi:https://doi.org/10.1016/j.pnucene.2020.103536.

[18] G. Bell. Probability distribution of neutrons and precursors in a multiplying assembly. *Annals of Physics*, 21(2):243–283, 1963. doi:https://doi.org/10.1016/0003-4916(63)90108-8.

[19] G. I Bell, W. A. Anderson, and D. Galbraith. Probability distribution of neutrons and precursors in multiplying medium, II. *Nuclear Science and Engineering*, 16(1):118–123, 1963. doi:https://doi.org/10.13182/NSE63-2.

[20] H. Hurwitz Jr., D. B. MacMillan, J. H. Smith, and M. L. Storm. Kinetics of low source reactor startups. Part I. *Nuclear Science and Engineering*, 15(2):166–186, 1963. doi:https://doi.org/10.13182/NSE63-3.

[21] H. Hurwitz Jr., D. B. MacMillan, J. H. Smith, and M. L. Storm. Kinetics of low source reactor startups. Part II. *Nuclear Science and Engineering*, 15(2):187–196, 1963. doi:https://doi.org/10.13182/NSE63-4.

[22] M. M. R. Williams. *Random Processes in Nuclear Reactors*. Pergamon, Oxford, 1 edition, 1974.

[23] R. Sanchez. An analysis of the stochasticity of the transport equation. *Transport Theory and Statistical Physics*, 26(4-5):469–505, 1997. doi:http://dx.doi.org/10.1080/00411459708017926.

[24] J. G. Hayes and E. J. Allen. Stochastic point-kinetics equations in nuclear reactor dynamics. *Annals of Nuclear Energy*, 32(6):572–587, 2005. doi:https://doi.org/10.1016/j.anucene.2004.11.009.

[25] U. Rohde, S. Kliem U. Grundmann, S. Baier, Y. Bilodid, S. Duerigen, E. Fridman, A. Gommlich, A. Grahn, L. Holt, Y. Kozmenkov, and S. Mittag. The reactor dynamics code DYN3D – models, validation and applications. *Progress in Nuclear Energy*, 86:170–190, 2016. doi:https://doi.org/10.1016/j.pnucene.2016.02.013.

[26] U. Rohde, M. Seidl, S. Kliem, and Y. Bilodid. Neutron noise observations in german KWU built PWRs and analyses with the reactor dynamics code DYN3D. *Annals of Nuclear Energy*, 112:715–734, 2018. doi:https://doi.org/10.1016/j.anucene.2017.10.033.

[27] M. Viebach, C. Lange, S. Kliem, C. Demazière, U. Rohde, D. Hennig, and A. Hurtado. Verification of the code DYN3D for calculations of neutron flux fluctuations. *Annals of Nuclear Energy*, 166:108735, 2022. doi:https://doi.org/10.1016/j.anucene.2021.108735.

[28] A. Vidal-Ferrandiz, S. Carlos, D. Ginestar, and S. Gallardo. Reduced model of a nuclear reactor and its use for teaching nuclear engineering courses. *Modelling in Science Education and Learning*, 12(2), 2019. doi:https://doi.org/10.4995/msel.2019.10806.

[29] International Atomic Energy Agency. Evaluated nuclear data file (ENDF), 2021. Last accessed October 2021. URL: https://www-nds.iaea.org/exfor/endf.htm.

[30] A. Fick. On liquid diffusion. *Philosophical Magazine*, 10(63):30–39, 1855. doi:https://doi.org/10.1080/14786445508641925.

[31] V. M. Piksaikin, A. S. Egorov, A. A. Goverdovski, D. E. Gremyachkin, and K. V. Mitrofanov. High resolution measurements of time-dependent integral delayed neutron spectra from thermal neutron induced fission of ^{235}U. *Annals of Nuclear Energy*, 102:408–421, 2017. doi:https://doi.org/10.1016/j.anucene.2017.01.001.

[32] G. R. Keepin. Delayed fission neutron data in reactor physics and design. In *Panel Proceedings Series: Delayed Fission Neutrons*, pages 3–22, Viena, Austria, 1967. URL: https://inis.iaea.org/search/search.aspx?orig_q=RN:43099306.

[33] Nuclear Energy Agency. Delayed neutron data for the major actinides, 2002. Last accessed December 2021. URL: https://www.oecd-nea.org/jcms/pl_13582/international-evaluation-co-operation-volume-6?details=true.

[34] Ž. Štacar, L. Barbot, and L. Snoj. Evaluation of the effect of burn-up on neutron flux and reaction rate distributions in the TRIGA Mark II reactor. In *PHYSOR 2016: Unifying Theory and Experiments in the 21st Century*, Sun Valley, United States, 2016. URL: https://hal.archives-ouvertes.fr/cea-02509717/.

[35] A. A. Nahla and M. F. Al-Ghamdi. Generalization of the analytical exponential model for homogeneous reactor kinetics equations. *Journal of Applied Mathematics*, 2012:1–12, 2012. doi:https://doi.org/10.1155/2012/282367.

[36] H. Fischer. *A History of the Central Limit Theorem: From Classical to Modern Probability Theory*. Springer, New York, 2011.

[37] J. F. C. Kingman. *Poisson Processes*. Oxford University Press, Oxford, 1993.

[38] C. Dubi and R. Atar. Modeling neutron count distribution in a subcritical core by stochastic differential equations. *Annals of Nuclear Energy*, 111:608–615, 2018. doi:https://doi.org/10.1016/j.anucene.2017.09.040.

[39] E. J. Allen, L. J. S. Allen, A. Arciniega, , and P. E. Greenwood. Construction of equivalent stochastic differential equation models. *Stochastic Analysis and Applications*, 26(2):274–297, 2007. doi:https://doi.org/10.1080/07362990701857129.

[40] E. J. Allen. A stochastic analysis of power doubling time for a subcritical system. *Stochastic Analysis and Applications*, 31(3):528–537, 2013. doi:https://doi.org/10.1080/07362994.2013.777287.

[41] A. Elsayed, M. El-Beltagy, A. Al-Juhani, and S. Al-Qahtani. A new model for the stochastic point reactor: Development and comparison with available models. *Energies*, 14(4):955–969, 2021. doi:https://doi.org/10.3390/en14040955.

[42] F. Vadillo. On stochastic models of chemical reactions. *Chemical Physics*, 549:111259, 2021. doi:https://doi.org/10.1016/j.chemphys.2021.111259.

[43] A. D. Fokker. Die mittlere energie rotierender elektrischer dipole im strahlungsfeld. *Annalen der Physik*, 348(5):810–820, 1914. doi:https://doi.org/10.1002/andp.19143480507.

[44] M. Planck. Über einen satz der statistischen dynamik und seine erweiterung in der quantentheorie. *Sitzungsberichte der Königlich Preussischen Akademie der Wissenschaften*, 24:324–341, 1917.

[45] M. Planck. Über die analytischen methoden in der wahrscheinlichkeitsrechnung. *Mathematische Annalen*, 104(1):415–458, 1931. doi:https://doi.org/10.1007/BF01457949.

[46] E. J. Allen. *Modeling with Itô Stochastic Differential Equations*. Springer, Dordrecht, 2007.

[47] R. Durrett. *Probability: Theory and Examples*. Cambridge University Press, Cambridge, 5th. edition, 2019.

[48] P. E. Kloeden and E. Platen. *Numerical Solution of Stochastic Differential Equations*. Springer, Berlin, 1992.

[49] J. M. S. Lubuma and A. Roux. An improved theta-method for systems of ordinary differential equations. *Journal of Difference Equations and Applications*, 9(11):1023–1035, 2003. doi:https://doi.org/10.1080/1023619031000146904.

[50] D. Suescún-Díaz, Y. M. Oviedo-Torres, and L. E. Girón-Cruz. Solution of the stochastic point kinetics equations using the implicit euler-maruyama method. *Annals of Nuclear Energy*, 117:45–52, 2018. doi:https://doi.org/10.1016/j.anucene.2018.03.013.

[51] M. Ossendrijver. Ancient babylonian astronomers calculated jupiter's position from the area under a time-velocity graph. *Science*, 351(6272):482–484, 2016. doi:https://doi.org/10.1126/science.aad8085.

[52] S. Q. Bogado Leite, M. T. de Vilhena, and B. E. J. Bodmann. Solution of the point reactor kinetics equations with temperature feedback by the ITS2 method. *Progress in Nuclear Energy*, 91:240–249, 2016. doi:https://doi.org/10.1016/j.pnucene.2016.05.001.

[53] MathWorks. Matlab (version 9.8), 2020. Last accessed December 2021. URL: https://www.mathworks.com/products/matlab.html.

[54] D. R. Ferguson and K. F. Hansen. Solution of the space-dependent reactor kinetics equations in three dimensions. *Nuclear Science and Engineering*, 51(2):189–205, 1973. doi:http://dx.doi.org/10.13182/NSE73-A26594.

[55] A. E. Aboanber, A. A. Nahla, and S. M. Aljawzneh. Fractional two energy groups matrix representation for nuclear reactor dynamics with an external source. *Annals of Nuclear Energy*, 153:108062, 2021. doi:https://doi.org/10.1016/j.anucene.2020.108062.

[56] A. E. Aboanber and A. A. Nahla. Adaptive matrix formation (AMF) method of space–time multigroup reactor kinetics equations in multidimensional model. *Annals of Nuclear Energy*, 34(1-2):103–119, 2007. doi:https://doi.org/10.1016/j.anucene.2006.07.012.

[57] A. E. Aboanber, A. A. Nahla, and N. M. Hassan. Probability distribution for neutron density of two energy group point kinetics system. *Annals of Nuclear Energy*, 119:300–309, 2018. doi:https://doi.org/10.1016/j.anucene.2018.04.041.

[58] A. E. Aboanber, A. A. Nahla, and Z. I. Al-Muhiameed. A novel mathematical model for two-energy groups of the point kinetics reactor dynamics. *Progress in Nuclear Energy*, 77:160–166, 2014. doi:https://doi.org/10.1016/j.pnucene.2014.06.016.

[59] M. Seidl, K. Kosowski, U. Schüler, and L. Belblidia. Review of the historic neutron noise behavior in german KWU built PWRs. *Progress in Nuclear Energy*, 85:668–675, 2015. doi:http://dx.doi.org/10.1016/j.pnucene.2015.08.016.

[60] G. Stein and C. Dubi. Stabilization of the stochastic point reactor kinetic equation through power feedback. *The European Physical Journal Plus*, 135(2):208, 2020. doi:https://doi.org/10.1140/epjp/s13360-020-00215-z.

[61] F. Vadillo. On the zero-neutron density in stochastic nuclear dynamics. *Dynamics*, 1(2):198–203, 2021. doi:https://doi.org/10.3390/dynamics1020012.

[62] Department of chemical and nuclear engineering, University of New Mexico. AGN-201M reactor operation and operator training manual, 1984. Last accessed January 2022. URL: https://www.nrc.gov/docs/ML2019/ML20195E222.pdf.

[63] W. B. H. Cooke. Predicted behavior of the ANG-201 reactor at high power levels. Master's thesis, U.S. Naval Postgraduate School, 1961. URL: http://hdl.handle.net/10945/12861.

[64] H. Taninaka, K. Hashimoto, and T. Ohsawa. An extended rod drop method applicable to subcritical reactor system driven by neutron source. *Journal of Nuclear Science and Technology*, 47(4):351–356, 2010. doi:https://doi.org/10.1080/18811248.2010.9711965.

[65] O. Novak, L. Sklenka, F. Fejt, I. Maldonado, and O. Chvala. Rod drop transient at VR-1 reactor – experiment and serpent transient calculation analysis. *Annals of Nuclear Energy*, 141:107296, 2020. doi:https://doi.org/10.1016/j.anucene.2019.107296.

[66] I. A. Kodeli. Sensitivity and uncertainty in the effective delayed neutron fraction (β_{eff}). *Nuclear Instruments and Methods in Physics Research A*, 715:70–78, 2013. doi:https://doi.org/10.1016/j.nima.2013.03.020.